André Filipe Peres Lúcio

Licenciado em Ciências de Engenharia de Micro e Nanotecnologias

Development of three - dimensional structures of yttria stabilized zirconia (YSZ) by lyophilization for biomedical applications

Dissertação para obtenção do Grau de Mestre em Engenharia de Micro e Nanotecnologias

Orientador: João Paulo Miranda Ribeiro Borges, Professor Doutor, FCT-UNL

FACULDADE DE CIÊNCIAS E TECNOLOGIA
UNIVERSIDADE NOVA DE LISBOA

Junho, 2017

Development of three-dimensional structures of yttria stabilized zirconia (YSZ) by lyophilization for biomedical applications

"Study hard what interests you the most,
in the most undisciplined, irreverent and
original manner possible."

Richard P. Feynman

Acknowledgements

First, I would like to express my deepest gratitude to my supervisor, Professor João Paulo Borges. Thank you for your attention, dedication, friendliness and for the full availability that was always shown to me.

To Eng. Nuno Neves, my intermediary between Innovnano and Departamento de Ciências dos Materiais, thank you for being always available to help me and to clarify me whenever it was necessary.

A special thanks to Eng. Andreia Lopes for having helped me in the data acquisition of the mechanical tests.

To everyone at CENIMAT, predominantly to the group coordinated by Professor Rodrigo Martins and Professor Elvira Fortunato for making SEM and XRD available for this thesis.

To all in the Departamento de Ciências dos Materiais (especially to those at the Laboratory 211), I would like to thank you all for having helped me and for maintaining a relaxed environment and a mutual support spirit.

To my best friends during these academic years: Ana Moleiro, André Nascimento, Daniel Elisiário, Gonçalo Salgado and Pedro Sousa. Thank you for your friendship, for all the confidences and the long (and constructive) talks that together we shared.

I would like to thank my family which has always supported me, and without which none of this would be possible and without which none of this would have the same magic. To them, I dedicate all this work.

To my Father, I would like to thank you for since I was a little boy you have aroused my curiosity to the themes of science and engineering; and because you have always been an example of what a real Man should be: a friendly son, a devoted husband, a comprehensive father and an honest and upstanding citizen.

To my mother, I want to thank her for the fact that she had unconditionally dedicated her life to their two children. For being always there…For being the example of a woman that throughout her life has faced great challenges but with a massive courage has always found hope for overcome them. Thank you for your dedication, support, affection and love.

Finally, I would like to thank my little sister Joana who since my 3 years old has rejoiced my life with her smile, her willingness and her *joie de vivre*.

A special kiss to my grandmothers.

Abstract

Over the last decade, zirconia has been widely used in biomedical applications, particularly in dentistry, because it exhibits an unique combination of advantageous properties: mechanical strength, low thermal conductivity, high density, low corrosion potential, biocompatibility, low cytoxicity and minimal bacterial adhesion. In particular, 3 mol% yttrium partially stabilized tetragonal zirconia (3YSZ) is known for presenting the highest strength and exhibiting transformation toughening which enhances fracture toughness. Additionally, in the recent years, nanocrystalline materials have received a great deal of attention, since they display unusual properties including higher strength and hardness.

Hence, in this study, a 3YSZ nanosized crystalline powder, provided by Innovnano, was applied as the starting material to produce quality solid foams using a freeze drying process followed by sintering. However, when dealing with nanopowders, processing problems rise due to nanoparticles agglomeration tendencies. This problem was mitigated by carrying out rheology studies to the powder's suspensions to determine the optimal viscosity for homogenous suspensions to be made.

Porous samples with densities between 1.95 g/cm^3 and 2.65 g/cm^3 and open porosities between 52.10% and 67.60% using a low sintering temperature (1350ºC) were obtained. These values lie above what is normal to obtain since it is difficult to manufacture highly porous foams of yttria-stabilized zirconia with porosity percentages greater than about 40 % to 50%. The morphological analysis of the samples was carried out using SEM and by means of X-ray diffraction, it was detected that the main crystallographic phase present in the porous samples is tetragonal (no T-M transformation occurred). By performing compression tests, porous samples with Young's modulus between 19.20 and 35.60 GPa and collapse stress between 62.60 and 73.20 MPa were obtained.

Keywords: 3YSZ, nanocrystalline, porous samples, lyophilization, rheology

Resumo

Ao longo da última década, a zircónia tem sido amplamente utilizada em aplicações biomédicas, particularmente em odontologia, porque apresenta uma combinação única de propriedades vantajosas: elevada resistência mecânica, baixa condutividade térmica, alta densidade, baixo potencial para sofrer corrosão, biocompatibilidade, baixa citotoxicidade e adesão mínima bacteriana. Em particular, a zircónia tetragonal parcialmente estabilizada com 3% mol ítria (3YSZ), é conhecida por apresentar uma resistência mais elevada e exibir uma propriedade denominada endurecimento por transformação (*transformation toughening)* que aumenta a sua tenacidade à fratura. Para além disso, nos últimos anos, os nanomateriais cristalinos têm recebido uma grande atenção, uma vez que exibem propriedades incomuns, incluindo maior resistência e dureza.

Deste modo, e neste estudo, foi utilizado um pó de 3YSZ nanométrico (fornecido pela empresa Innovnano) como material de base para produzir espumas sólidas de qualidade utilizando um processo de liofilização seguido de sinterização. No entanto, ao lidar com nanopós, os problemas de processamento aumentam devido á tendência das nanopartículas para agregarem. Este problema foi atenuado ao realizar estudos de reologia às suspensões de pó para determinar a viscosidade ótima para obter suspensões homogéneas.

Foram obtidas amostras porosas com densidades entre 1,95 g/cm^3 e 2,65 g/cm^3 e porosidades abertas entre 52,10% e 67,60% com uma baixa temperatura de sinterização (1350ºC). Estes valores situam-se acima do que é normal obter, uma vez que é difícil fabricar espumas altamente porosas de zircónia estabilizada com ítria com percentagens de porosidade superiores a cerca de 40% a 50%. A análise morfológica das amostras foi realizada utilizando SEM e por meio de difração de raios X, foi detetado que a fase cristalográfica principal presente nas amostras porosas é tetragonal (não ocorreu envelhecimento, i.e., transformação T-M). Ao realizar ensaios de compressão, foram obtidas amostras porosas com módulos de Young entre 19,20 e 35,60 GPa e tensões de colapso entre 62,60 e 73,20 MPa.

Acronyms

CAD/CAM	Computer-Aided Design/ Computer-aided manufacturing
T-M	Tetragonal to monoclinic phase transformation
Mg – PSZ	Magnesium partially stabilized zirconia
Y-TZP	Yttria stabilized tetragonal zirconia polycrystal
ZTA	Zirconia-toughened alumina
NsM	Nanostructured material
CUF	Companhia União Fabril
3YSZ	3 mol % yttria partially stabilized tetragonal zirconia
EDS	Emulsion Detonation Synthesis
AOT	Dioctyl Sulfosuccinate Sodium salt
PVA	Polyvinyl alcohol
M.W.	Molecular Weight
TMAH	Tetramethylammonium hydroxide
SEM	Scanning Electron Microscope
MSC	Mesenchymal cells
SOFCs	Solid Oxide Fuel Cells
TBCs	Thermal barrier coatings
XRD	X-Ray Diffraction

Symbols

wt%	Weight percentage
λ	Wavelength
h_0	Initial height
d_0	Initial diameter
V_0	Initial volume
p_o	Open porosity
p_c	Closed porosity
ε	Mechanical strain
Ϭ	Mechanical stress
E	Young's Modulus (or Elastic modulus)
$\left(\frac{\rho}{\rho_s}\right)$	Foam's relative density
ρ	Foam's density
$\boldsymbol{\rho_s}$	Density of the solid
$\boldsymbol{E_s}$	Material's Young's Modulus
$\boldsymbol{\sigma^*_{pl}}$	Collapse stress
$\boldsymbol{\sigma_y}$	Bending strength
$\boldsymbol{\sigma^*_{pl\,min}}$	Minimum collapse stress
$\boldsymbol{\sigma^*_{pl\,max}}$	Maximum collapse stress
$\boldsymbol{\sigma_{y\,min}}$	Minimum bending strength
$\boldsymbol{\sigma_{y\,max}}$	Maximum bending strength
V_T	Total volume of the sample
$V_{s,}$	Volume of the solid
V_{po}	Volume of the open pores
V_{pc}	Volume of the closed porosity

$\rho_{t,}$	Theoretical density
m_1	Mass of the solid
m_2	Impregnated mass
m_3	Mass while immersed
V_a	Apparent volume
ρ_{H_2O}	Water density
P_c	Percentage of closed porosity
P_o	Percentage of open porosity

Table of contents

Figure Index

Table Index

1- Introduction

George Bernard Shaw, an irish playwriter once wrote that: "*The reasonable man adapts himself to the world; the unreasonable one persists in trying to adapt the world to himself. Therefore all progress depends on the unreasonable man."* And this is the reason why, over the last decades, unreasonable men and women that comprehend the scientific community have been developing products (sometimes supported by the industry) with the main objective of substitute living tissues (or at least a part of them) in animal organisms.

With this purpose, there have been created and tested materials that show favorable characteristics of compatibility and integration with the living tissues, preventing reactions (or even the rejection) by the immune system of the organisms. These materials are called biomaterials. According to the journal Nature, biomaterials can be defined as *"those materials — be it natural or synthetic, alive or lifeless, and usually made of multiple components — that interact with biological systems. Biomaterials are often used in medical applications to augment or replace a natural function."*[1] These materials may be formed by metals (or alloys), ceramics, polymers or composites. However, in this dissertation, we will be focusing on bioceramics. As the name suggests, bioceramics are materials based on ceramics that have been widely used in coating on metallic implants and in dentistry to repair/ rebuild parts of the dental arch that have been infected or even destroyed. When compared with other types of biomaterials, the main advantage of the bioceramics is the fact that they are highly biocompatible (typically these materials do not induce reactions on the host tissues). Plus, they are corrosion resistant and present high compressive strength. However, these materials show high density and are brittle, which limits their application; particularly in situations where the loads applied affect their performance. [2]

In 1952, a swedish orthopedist named Per-Ingvar Brånemark discovered while studying blood flow in rabbit's legs that by introducing titanium in their femur, the metal would became deeply bonded with the bone. [3] With this discovery came up the concept of osseointegration (direct contact between a living bone and an artificial implant) and that was the starting point of today's dentistry implants industry. Originally, the first titanium dental implants inserted by Brånemark in 1981 [4] and the one's still used today can be divided in three parts: fixture (considered as the artificial tooth root, it is below the gingiva line and it is implanted and fused with the mandible), abutment (part that supports the crown and that lies at and above the gingiva line) and crown (the replacement tooth custom made to match the natural teeth colour). Since then, titanium and titanium alloy implants continue to be conventionally used in implant dentistry because of their mechanical and biocompatibility properties.

However, titanium is a metal and in the oral cavity we can find water in the form of saliva. Plus that, the mouth is exposed to changes on its pH and temperature. These factors and also the presence of microorganisms can lead to the corrosion of titanium/ alloy implants and consequently to their mechanical failure. [5] Therefore, corrosion products can be formed (mostly titanium ions and microparticles of titanium) which may diffuse to adjacent tissues of the gingiva serving as an additional cause of rejection. [6] Actually, titanium can cause allergic reactions (facial erythema and edematous) [7] and not only concentrate in the adjacent tissues of the gingiva line but also in the lymph nodes or in the pulmonary tissues. [8-10] Furthermore, and since titanium is a high thermal conductor metal, it was shown that the implant contact with hot fluids can be damaging to healing tissues surrounding the implant.[8] Additionally, titanium abutments can create an unaesthetic aspect since there is grey metal showing through the mouth. To overcome these problems, ceramic biomaterials started to be considered since they are made of inorganic non-metallic oxides. Plus, they offer high biocompatibility, low corrosion potential, low thermal conductivity [11] and they can improve the appearance of oral implants since they present a colour similar to the teeth. Besides, dental plaque has a less probability to grow and accumulate in ceramic materials than in metal substrates. [12]

Aluminum oxide (commonly called alumina) and zirconium dioxide (also known as zirconia) are bioinert ceramics which means that these materials are less predisposed to cause an hostile biological reaction due to their chemical stability compared to other materials. [13] Moreover, their low reactivity together with their good mechanical properties led to their use in dental devices. In 1982, an implant totally made of alumina (99, 7%), the Tübinger implant, [14] was developed but it was later removed from the market. Even though it showed good levels of resistance under compression, under tensile strength it was fragile. Additionally, at a room temperature, alumina fractures without showing plastic deformation and once fracture starts it progresses rapidly. [13,15]. Besides, other studies using different aluminium oxide systems found less- bone implant contact compared to titanium and reduced survival rates. [16, 17]

Zirconium oxide (ZrO_2) has been widely used in dentistry because of its advantageous physical, chemical, biological and aesthetical properties. The unique combination of mechanical strength, low thermal conductivity, high density, low corrosion potential, biocompability, low cytoxicity and minimal adhesion of bacteria made zirconia become one of the top restorative choices. Nowadays, this material has been widely adapted to a number of dental uses: endosseous implant fixtures, abutments for endosseous implants and ceramic crowns. When applying zirconia as an endosseous implant fixture, different studies have categorically shown the capability of zirconia to integrate with the maxilo-facial bone and that osseointegration success is comparable with the one achieve using titanium, namely soft-tissue attachment for zirconia is comparable to the titanium alloys. Also, zirconia stimulates the attachment of human gingival fibroblasts *in vivo*, forming the junctional epithelium. [18- 23] Zirconia biocompatibility and its osseointegration *in vitro* have also been examined in several studies. The results detected no cell toxicity from the zirconia to the osteoblasts. On the contrary, it promotes proliferation of osteoblasts at greater levels than alumina. [24] Similar *in vitro* studies testing the biocompability of zirconia to fibroblasts concluded that zirconia is not cytotoxic. [25]

Additionally, in order to assess biocompatibility to osteoblasts and fibroblasts, zirconia *in vitro* testes using different immune cell lines (e.g. lymphocytes, macrophages) also shown any significant cytotoxicity. [24] Other studies *in vitro*, concluded that zirconia is less prone to maintain bacterial biofilms that titanium. [26] Besides hard tissue, the biological response of the peri-implant soft tissues has also been assessed in different studies. Peri-implant health was found favourable for zirconium oxide implants. The clinical soft tissues parameters around zirconia implants, including probing depth (indication of bone support loss), clinical attachment level, bleeding index, and plaque index (indication of biofilm accumulation) were comparable to those around titanium implants. [27-31]

When zirconia is applied as an abutment for endosseous implant, *in vitro* investigations have concluded that the adhesion and proliferation of fibroblasts and epithelial cells in zirconia are comparable and sometimes superior to titanium. [32, 33] This characteristic of the abutment it is crucial to enable the connection/ proliferation of fibroblasts and epithelial cells, reducing the creation of bacteria/ biofilms. It was also shown that the connective tissue attachment around the zirconia abutments for, a more stable mucosal seal than the gold abutments. [34] Different medical studies were conducted to evaluate the performance of zirconia implant abutments. Periodontal disease indexes including plaque index, bleeding on probing and probing depth were evaluated and compared with titanium abutments [35, 36].

As already referred, one of the major reasons to develop zirconia abutments is the fact that they can improve the appearance of oral implants since they present a colour similar to the teeth. The principal statement has been that the white colour of zirconia would cause less colour change in the nearby soft tissues than the grey colour seen in these tissues when using titanium abutments. An animal study has stated that zirconia implant abutments definitely discolour the mouth less than titanium. [37]

Zirconia was first used in dentistry as the main material for ceramic crowns. The development of CAD/CAM technologies has allowed the fast and accurate manufacture of zirconia crowns. When compared with the conventional alloy-ceramic crowns, zirconia crowns have comparable clinical success rates. Yet, the low success in molar regions related to the heavily loading bite force, has been a concern. [38]

Depending on temperature, pure zirconium oxide subsists in three different crystal phases' structures: monoclinic, tetragonal and cubic [39, 40] which are represented in Figure 1. At room temperature, the most stable phase is the monoclinic. Above 1170ºC, it starts the phase transformation from monoclinic to the tetragonal phase. After heated above the 2370ºC, zirconia undergoes other phase transformation from tetragonal to cubic phase which stands until zirconia's melting point. [41]

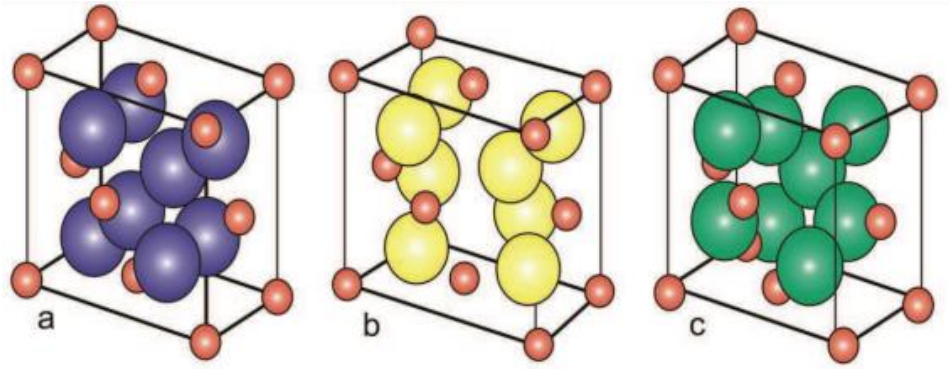

Figure 1 – The three different crystal phases' structures of zirconia: **(a)** monoclinic, **(b)** tetragonal and **(c)** cubic zirconia. [42]. © 2011 Maziero Volpato C Â, D´Altoé Garbelotto LG, Fredel MC, Bondioli F. Published in Advances in Ceramics - Electric and Magnetic Ceramics, Bioceramics, Ceramics and Environment under CC BY-NC-SA 3.0 license. Available from: http://dx.doi.org/10.5772/21630

As referred before, zirconia has been widely used in dentistry and medicine. However, the use of pure zirconia is inadequate due to the spontaneously phase transformation from tetragonal to monoclinic crystal structure (commonly known as T-M transformation). When this transformation happens (during zirconia cooling after sintering), there is a 4-5% volume increase that causes a loss in density and a reduction in strength and toughness, since the crystal lattice becomes more firm and cannot put up with the expansion, promoting a persistent crack propagation and ultimately leading to prosthesis failure. This degradation process is called ageing and is caused by the progressive and spontaneous transformation of the tetragonal phase into the monoclinic phase. [43-47] With the objective to decelerate or abolish these changes in the crystal structure of zirconia, several oxides such as MgO (magnesium oxide), CaO (calcium oxide) and Y_2O_3 (yttrium oxide or yttria) have been used to dope zirconia. [48] Stabilization of the tetragonal phase can be achieved by replacement of some Zr^{+4} ions with some larger ions such as Mg^{2+} or Y^{3+}. This property is called transformation toughening and near this metastable tetragonal phase, the dopant effect will promote the T-M transformation which will permit a local expansion which will put the forming crack into compression and stop the development of the crack, enhancing fracture toughness. [49]. Transformation toughening is a major asset to biomedical applications, where crack propagation is almost always a major clinical liability.

There are 3 major types of zirconia that have being used in biomedical applications: magnesium partially stabilized zirconia (Mg – PSZ), yttria stabilized tetragonal zirconia polycrystal (Y-TZP) and zirconia-toughened alumina (ZTA). Yet, most progresses were achieved using YTZP. This ceramic is formed by tetragonal submicron-sized grains, which is today the most used bioceramic for dental applications. [15] At room temperature, the rate of Y-TZP retained in the tetragonal phase is influenced by [13]: the homogeneity and grains size, the concentration of the oxide that

stabilizes yttria and the constriction applied by the crystal matrix into the grains. The balance between these crystallographic parameters influences the mechanical properties of Y-TZP ceramics.

Y-TZP has the highest strength and toughness among zirconia ceramics exhibiting a remarkable flexural strength, a prominent fracture toughness which reduces ageing degradation and has allowed applying it in the implant dentistry field. [50, 51] Hisbergues *et al.* has concluded that the mechanical strength of Y-TZP implant is sufficient to survive masticatory forces that are commonly encountered by endosseous implants. [52] The strength degradation can be controlled by having a high density, small and uniform grain size and a spatial gradient of yttria concentration within grains. These parameters are controlled by the manufacturing method and the precursors choose for the ceramic's production. [18] However, the best results can be achieved when using nanostructured 2% to 3% mol yttria stabilized zirconia. The use of percentages superior to 8% mol Y_2O_3, form a suspension totally stabilized with a monoclinic crystal structure making it not appropriate for dental implant applications. [53]

It is important to explain that a nanostructured material (NsM) can be defined as a physical substance with at least one external dimension with a size range between 1 and 100 nanometers. [54] These materials have received a great deal of attention, in the recent years, since they exhibit quite dramatic effects (particularly increasing strength) on the bulk material when their molecular structure is changed and their size is reduced. For example, when the grain's size of nanocrystalline ceramics is reduced they become more malleable/ flexible. [55] This superelasticity is followed by improved toughness, enhanced ability to bond with metallic components and increased wear resistance. In nanocrystalline ceramics, superelasticity (deformation beyond the normal breaking point) can be observed by grain boundary sliding. [56] Furthermore, they can exhibit very high magnetoresistance (great reduction in electrical resistance when an external magnetic field is applied) and superparamagnetism (the magnetic moment of the nanomaterial can be considered as composed by the individual magnetic moments of the atoms which compose the nanomaterial) properties. [57] Besides, and since the grain size is smaller than the light wavelength these nanocrystalline ceramics can show transparency. [58] Other advantages include extremely low thermal conductivity, reduction of the sintering temperature (reducing the shrinking size significantly) and increased reactivity because of the increased surface area. [59]

In this dissertation, we will be using a 3 mol % yttria partially stabilized tetragonal zirconia powder to produce porous foams. This powder was supplied by Innovnano – Materiais Avançados S.A. which is a company part of the CUF group (Companhia União Fabril) established in 2003, in Aljustrel, and based in Lisbon. This company develops its activity on the production and marketing of ceramic nanomaterials, including 3YSZ (3 mol % yttria partially stabilized tetragonal zirconia), based on its own synthesis process of micro and nanoparticles developed in-house and patented in 2008, called EDS (Emulsion Detonation Synthesis). This technique ensures that powders are produced with a higher quality and consistency, offering a more reactive nanostructure, greater stability of the zirconia phase, greater chemical homogeneity and a uniform distribution of yttria. [60] These materials may be used for medical and dental implants or used as thermal barriers.

As manufacturing process, we will use freeze drying (also known as lyophilization) to produce porous foams of Y-TZP. This process has been widely used in pharmaceutical and biotechnology industries. [61] When used has a manufacturing process for ceramic materials, compact green bodies can be achieved as also controlled porous size. This technique is extremely versatile since it allows to shape and create porous structures in the same process using ice crystals as porogens. It consists on depositing aqueous colloidal suspensions of ceramics in an atmosphere below the water's freezing point [62, 63] controlling the ice growth by the temperature, the freezing device or by the cooling rate. During the ice growth, the frozen crystals morphology can be modified by the addition of solvents (e.g. binders, salts) to create different pores structures. [64-67] Once the

samples are entirely frozen, they are exposed to a sublimation process to remove the frozen solvent and leave porous structures behind, which matches the volume previously occupied by the frozen solvent. The green samples are then sintered to strengthen and compact the foams. In this dissertation, the linear and volumetric contraction as well the mechanical properties of the samples will be studied.

Since we will handle with a nanostructured ceramic powder, with an average particle size of 60 nm, major obstacles come along including the strong predisposition of nanocrystalline powders to agglomerate. In particular, the agglomeration of nanopowders can be problematic for different reasons. These nanoparticles have a large surface area and so they have the tendency to agglomerate to minimize the total surface area or interfacial area of the system. And so, a uniform dispersion of nanopowders is required to achieve the desired product characteristics. Also, non-uniformity will affect the pore-size distribution in the resulting green body and, consequently, the sintering behavior of the compacted particles, possibly leading to grain size heterogeneities. [68,69]

The knowledge of the interaction forces between the nanoparticles are important because they control colloid behavior such as viscosity and yield stress, particle packing (green density) under applied pressure, and interaction of particles with other interfaces. Strong attractive van der Waals forces acting between the particles are the driving force of the agglomeration producing high viscosity, paste-like suspensions with yield stresses, low green density due to inefficient particle packing under applied pressures [70] and aggregated rapidly settling suspensions.[71] Repulsion between particles produces dispersed suspensions that have low viscosity, pack to high and uniform green density under applied pressures and remain stable against sedimentation if colloidal in size.[72] This has to be overcome if a high quality nanoceramic is to be produced; a general practice in dealing with this issue is to create a stable suspension, in which all particles repel each other. This is achieved through the use of dispersing agents and adjusting the pH [73, 74]. The optimum pH or amount of dispersant to create a stable suspension can be experimentally found through rheological measurements. And so, it was studied the optimization of the amount of dispersant on the suspensions of 3YSZ used in the process of lyophilization to produce the porous ceramic foams.

Throughout rheological measurements the flow behavior is examined in a reaction to an applied shear stress. A crucial rheological parameter is the viscosity of suspensions. Rheological measurements are required to describe the properties of colloidal suspensions, specifically are used in order to determine the optimal amount of dispersant necessary to stabilize a suspension. This is done by evaluating the viscosity of a suspension against changing dispersant concentrations [75]. The viscosity of the 3YSZ suspensions was also studied.

It is important to mention that *in vitro* and *in vivo* studies to evaluate the influence of water in their stability were not performed and must be considered in future works. For application as biomaterials cytotoxicity studies must also be considered in the future, despite the reports on zirconia biocompatibility available in the literature.

2 – Materials and Methods

The experimental work of this dissertation involved the production of porous foams of 3YSZ using a freeze drying (lyophilization) process followed by sintering. This chapter briefly describes the materials, procedures and characterization techniques used to produce and characterize the porous foams.

2.1 – Lyophilization of 3YSZ porous foams

The preparation of 3YSZ porous foams was carried out according to the following procedure and using the materials described below.

2.1.1 – Materials

Innovnano supplied a 3 mol % yttria partially stabilized tetragonal zirconia powder with an average particle size of 60 nm. Furthermore, dioctyl sulfosuccinate sodium salt (AOT, Sigma-Aldrich, ≥ 97%) was used as a surfactant and polyvinyl alcohol (PVA, 95% hydrolyzed, M.W. 95000, and ACROS Organics) as a binder. All the reagents were used as received without any further purification.

2.1.2 – Procedure

A 4 w/w% aqueous solution of PVA was prepared to act as a binder. This solution was prepared by dissolving 4 g of PVA in 100 mL of water. Stirring and heating was required since PVA is difficult to dissolve. To optimize the manufacturing method of the fine structure of the 3YSZ porous foams, the amounts of 3YSZ, PVA and surfactant were changed to produce different slurries as shown in Table 1.

At first, the aim was to compare the characteristics of the porous samples with the codes A and B, differentiating the percentage of 3YSZ (w_{3YSZ} / w_{Total}) while maintaining the percentage of AOT (w_{AOT} / w_{3YSZ}). Then, we tried to compare the characteristics of the specimens with codes B, C, D and E by keeping the percentage of 3YSZ and changing the percentage of AOT.

Table 1 - Chemical composition of the yttrium slurries.

Samples' Group Code	% 3YSZ (w_{3YSZ}/ w_{Total})	Binder – PVA (mL)	% AOT (w_{AOT}/w_{3YSZ})
A	28	5	4
B	40		4
C			10
D			15
E			20

To obtain homogeneous slurries, an IKA T10 basic ULTRA TURRAX disperser was used. After homogenization, the liquid suspensions were place inside the wells of a 48-well plate. Then, the plate was placed in a refrigerator for 24 hours with the intent of removing bubbles and prepare the samples for lyophilization which was carried out using a bench top manifold freeze dryer (Zirbus Technology, VaCo2). Before lyophilization, the plate was immersed into liquid nitrogen. In this step, it is important to freeze the liquid to a temperature below its triple point. It is the most critical stage for obtaining porous foams with good morphological characteristics.

However, it was found that the results were not consistent (as concluded on Chapter 3) and it was needed to do some further research on our method of producing the ceramic suspensions.

And so, the viscosity of the suspensions was optimized (reduced) in order to allow a better treatment/ stabilization and to avoid the presence of air bubbles upon freezing and prior to lyophilization. Therefore, suspensions of 40% and 50% 3YSZ (w_{3YSZ}/ w_{Total}) were prepared as shown in Table 2.

Table 2 - Chemical composition of the optimized slurries.

Samples' Group Code	% 3YSZ (w_{3YSZ}/ w_{Total})	% PVA (w_{PVA}/w_{3YSZ})	% AOT (w_{AOT}/w_{3YSZ})	%TMAH (w_{AOT}/ w_{3YSZ})
F	40	5	2.5	6.7
G	50			

A 9 w/w % PVA solution in water was prepared and to each suspension a certain amount of this solution was added to ensure that in the final suspension 5% (w_{PVA}/w_{3YSZ}) PVA is present. For example, sample F was prepared using: 3 g of 3YSZ; 1.67 g of a 9% aqueous solution of PVA; 0.2 g of TMAH and 0.075g of AOT. Final content of 3YSZ in the suspension (w_{3YSZ}/w_{Total}) was adjusted by addition of 2.5 mL (2.5 g) of water. The percentage of AOT (w_{AOT}/w_{3YSZ}) was reduced to 2.5% because it was found that even with a percentage of 4%, there was stabilization of air bubbles in the suspensions that were impossible to eliminate, giving rise to uncontrolled porosity (heterogeneity), such as explained on Chapter 3. TMAH (Tetramethylammonium hydroxide) was used since it was shown that it enhances the stabilization of ceramic colloidal systems. [76]

Additionally, rheology studies were carried out using a Bohlin Gemini HRnano rheometer to study viscosity since it is necessary to obtain low viscosity suspensions of nanosized particles to produce solid foams with controlled porosity.

2.2 – Sintering

Sintering is an agglutination process of ceramic solid particles that occurs by heating them at temperatures below its melting temperature. It was used a Nabertherm LT 9/11SKM oven and the heating cycle employed is shown in Figure 2.

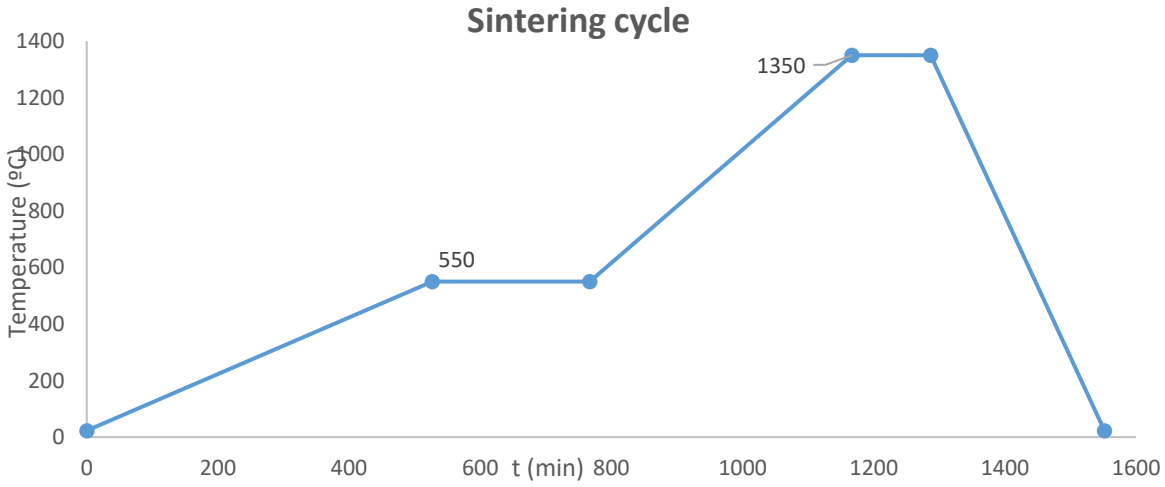

Figure 2 – Heating cycle used to produce the 3YSZ porous foams.

2.3 – 3YSZ porous foams characterization

2.3.1 – Dimensional analysis

The dimensions of the cylindrical porous foams were measured after the process of lyophilization and after sintering. With this analysis, it was possible to evaluate the linear and volumetric contraction of the samples.

2.3.2 – Archimedes method density measurement

The determination of the density and porosity of the 3YSZ porous foams was performed using the Archimedes method. The mass of each sample was weighed on air. This mass was referred to as dry mass. After that, the mass was measured while the sample was suspended in water. This is referred to as the suspended mass. Then the sample was lightly rubbed dry and weight in air. This was called the wet mass. For further details on the technique please see the supporting information in annex.

2.3.3 – Morphological analysis using SEM

The analysis of the morphology of the 3YSZ porous material was performed using a high-resolution scanning electron microscope (SEM, model Zeiss AURIGA). The samples' observation required a careful preparation: firstly, the samples were placed in a rack on carbon tape and covered with gold using a sputter coater. Subsequently, the sample holder was inserted into the equipment's observation chamber under vacuum, followed by observation of the samples.

2.3.4 - Determination of crystalline phases using X-ray diffraction technique

A sample of 3YSZ was characterized by X-ray diffraction (X'PerPRO, PANalytical) with CuKα radiation ($\lambda = 1.540598$ Å). The diffraction pattern was collected in Bragg-Brentano configuration in 2θ ranging from 20° to 90° at a scanning rate of 0.0334º.

2.3.5 – Compression tests

Compression tests were performed using 80 cylindrical test pieces in a universal testing machine (Shimadzu AG) with a load cell of 50 kN.. The load was applied to the sample at a speed of 0.5 mm /min.

3 – Results and Discussion

3.1 – Dimensional analysis

The 3YSZ ceramic porous foams after the lyophilization procedure, and as shown in Figure 3a), acquired a fragile aspect since the ceramic material which constitutes them is weakly bounded. This inherent fragility will depend on the percentage of 3YSZ, PVA and surfactant that were used to produce the different types of colloidal suspensions. These green bodies have a cylindrical shape which results from the fact that the ceramic colloidal suspensions were placed inside the wells of a 48-well plate. As shown in figure 3b), after the heating cycle, the result of this heat treatment was an increase in samples density (densification) which has a practical purpose since there is a reduction of porosity, shrinkage and consequently an increase of mechanical strength.
All this happens because before sintering, the particles surface area of the samples has a high concentration of structural defects and broken bonds. When compared with the interior of the crystal structure, the surface energy is much higher. With an increase of temperature, occurs an consolidation process which leaves the system a lower energy state that combines with the conversion of many particles of small dimensions in bigger particles, substituting gas-solid interfaces by solid-solid interfaces, which means, an increase in density and consequently shrinkage.

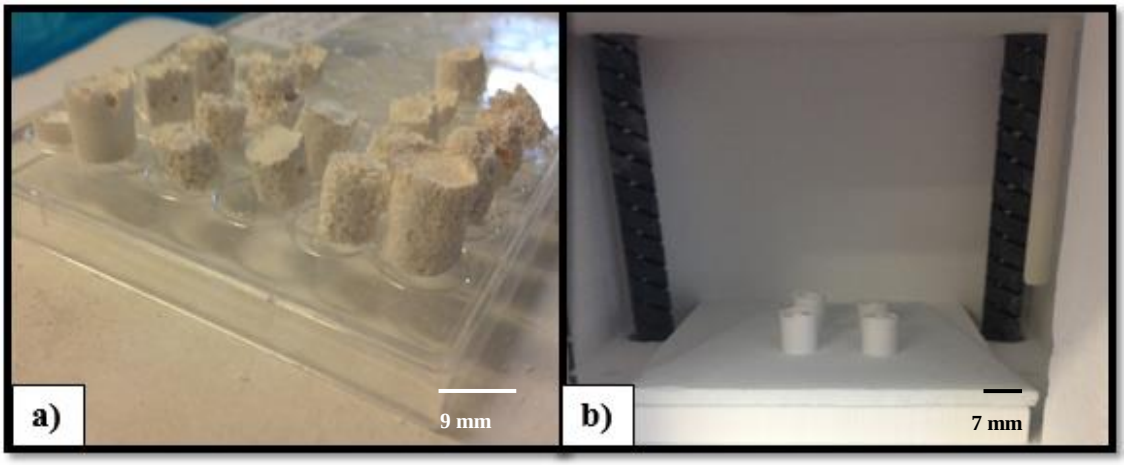

Figure 3 – 3YSZ porous foams **a)** after lyophilization process and **b)** after the heating cycle. The photos were captured using an iOS iPhone 6s. Photos by: André Lúcio

With the propose of evaluating the linear and volumetric shrinkage of the samples, right after the process of lyophilization, the height (h_0), diameter (d_0) and the volume (V_0) of each green body was measured. After sintering, the procedure was repeated. Consequently, the results of the linear and volumetric contraction for the samples with 40% and 50% 3YSZ (w_{3YSZ}/ w_{Total}) (samples F and G) are presented on Table 3, respectively. This analysis was only performed for these two samples because these are the ones where optimization of the ceramic suspension was performed.

Table 3 – Linear and volumetric contraction of 3YSZ samples.

% 3YSZ (w_{3YSZ}/ w_{Total}) on the sample	**$\Delta h/h_0$ (%)**	**$\Delta d/d0$ (%)**	**V_0 (cm^3)**	**V (cm^3)**	**$\Delta V/V_0$ (%)**
40	-25.76 ± 9.19	-27.41 ± 3.83	1.57 ± 0.65	0.61 ± 0.26	-60.62 ± 7.58
50	-25.10 ± 2.75	-26.48 ± 1.00	1.03 ± 0.04	0.42 ± 0.02	-59.51 ± 1.90

These results prove that during the sintering process, both the 40% and 50% 3YSZ samples exhibited a linear and volumetric isotropic contraction. It means that the agglutination of the particles that occurred during this process, approximately equally altered the length, the diameter (and hence the volume) of the cylindrical samples. This also shows that the homogenization of the colloidal suspensions that served as the basis for the production of the samples, was carried out successfully. Furthermore, it is possible to see that contraction, either linear or volumetric, is independent on the amount of solids. Since the porosity decreases with the amount of solids present in the suspensions (see section 3.2 - Density and porosity), these results suggest that the size of the pores has decreased. SEM analysis (section 3.4 - Morphological analysis) seems also to confirm this assumption.

These outcomes are important because while sintering not only the samples dimensions change but also their shape as a consequence of anisotropic sintering shrinkage. The occurrence of shrinkage anisotropy is an important practical issue in the fabrication of ceramics by sintering. For example, anisotropic shrinkage behavior can cause formation of undesired cavities and other microstructural damages. [77]

3.2 – Density and porosity

Density and porosity (also called void fraction) have an enormous influence on the final properties of ceramic samples after sintering which will directly affect the final applications that we can give to these materials. Two types of porosity can be differentiated: open and closed porosity. Open porosity (also called effective porosity), Po, refers to the fraction of the total volume of the sample that can be theoretically occupied with a fluid. On the other hand, closed porosity (or ineffective porosity), Pc, refers to the fraction of the total volume of the sample in which fluids flow can't effectively occur and also to the pores isolated inside the samples that tend to assume a spherical form.

Porosity and density measurements were performed based upon Archimedes principle. The mass of each sample was weighed on air. This mass was referred to as dry mass. After that, the mass was measured while the sample was suspended in water. This is referred to as the suspended mass. Then the sample was lightly rubbed dry and weight in air. This was called the wet mass. This enabled the determination of the bulk density and open/closed porosity using the equations derived in the Support Information in annex in particular "Archimedes or immersion method for determination of porosity".

The presence of pores in the samples is required because it is through them that osteoblasts (major cellular components of bone) and mesenchymal stem cells (MSCs) migrate and proliferate into the surrounding bone tissue. This will enhance vascularization and consequently develop bone ingrowth and a greater mechanical stability between the implant and the bone. [78] Hence, it is expected that a higher porosity will enhance osteogenesis since it will result in an increase in cell proliferation and simplify the transportation of oxygen and nutrients (and different studies have shown it). Furthermore, a porous interconnected structure is vital to permit the diffusion of waste products out of the samples, and the products that come with samples degradation should be able to be removed without interference with other organs and surrounding tissues.

The porosity of yttria stabilized zirconia ceramics has been widely studied since this material has not only being used for biomedical applications but also as a structural component in solid oxide fuel cells (SOFCs), gas sensors and thermal barrier coatings (TBCs). [79-81] Depending on their application, the manufacturing process must be optimized to achieve the different required properties, such as pore size, porosity or microstructure.

The values of density, open and closed porosity of the sintered samples are presented in Table 4.

Table 4 - Variation of the porosity (open and closed) and density.

Samples' s Group Code	Density (g/ cm^3)	P_o (%)	P_c (%)
A	1.21 ± 0.05	70.00 ± 1.00	10.00 ± 4.00
B	1.39 ± 0.07	59.00 ± 11.00	20.00 ± 10.00
C	1.87 ± 0.09	54.00 ± 13.00	15.00 ± 13.00
D	1.65 ± 0.30	60.00 ± 3.00	13.00 ± 4.00
E	1.48 ± 0.05	39.00 ± 12.00	36.00 ± 13.00
F	2.03 ± 0.08	65.60 ± 2.00	2.10 ± 0.06
G	2.62 ± 0.03	53.00 ± 0.90	3.90 ± 0.05

By analyzing the results of the samples with the groups code A, B, C, D and E, it is possible to verify that there is a huge dispersion of values of density and porosity. This dispersion is the result of the presence of pores created by air bubbles trapped in the porous foams' structure as can be seen in section 3.4 - Morphological analysis. These pores are caused by the fact that upon homogenization of the colloidal suspensions, the dispersant used is responsible for the stabilization of air bubbles which after lyophilization and sintering gave rise to spherical pores. Thus, it was necessary to perform rheological studies, to study the viscosity of the suspensions in order to prevent the stabilization of these air bubbles. The result was the production of the samples with code F and G. And so, it was possible to obtain porous foams with densities between 1.95 g/ cm^3 and 2.65 g/ cm^3 and open porosities between 52.10% and 67.60%.

We must take into account that the processing method has a decisive influence on the degree of porosity of the ceramic products. For example, Kim H *et al*. were able to achieve highly porous YSZ samples with porosities superior to 75% using tape casting. Although the values that we achieved are lower relatively to this one's, the truth is that they lie above what is normal to obtain since it is difficult to manufacture highly porous foams of yttria-stabilized zirconia with porosity greater than about 40 % to 50%. [82] Furthermore, we obtained better results that the one's achieved by Yunfeng Gu *et al*. that developed YSZ porous ceramics with open porosities between 33.1–50.3% using gelcasting as manufacturing method and a minimum loading of 50 vol% of solids. [83] Gelcasting was also used by Liang Fa Hu *et al*. to produce porous YSZ ceramics with high porosities but this time using low solid loadings of 10% and 15% obtaining values of porosity between 70 and 76%. [84]

Additionally, freeze casting has also been used to fabricate highly porous yttria-stabilized zirconia with porosity varied between 67% and 82% [85]. Even though our results in terms of porosity are lower, it is possible to sustain that with the manufacturing process that we used it is possible to obtain highly porous 3YSZ ceramics. Also, freeze drying has been widely studied and used in the production of bioceramics permitting to create different rates of porosity and morphologies. Besides, this method is simple, low cost and can be easily improved to current companies processing methods with low resources investments. Moreover, it is also applicable to many other ceramic systems. In addition, PVA was used as a binder to suppress ice crystals growth reducing the pore's size substantially.

Liang Fa Hu. *et al.*, investigated the influence of sintering temperature on compressive strength of porous YSZ through measurements of pores size, porosity and linear shrinkage. They showed that by using a sintering temperature of 1350ºC, as it was used in our heating cycle (by Innovanano's advice), it was possible to obtain porous YSZ ceramics with open porosities of 77%. However, they also showed that compressive strength increased with the rise of sintering

temperature from 1350 to 1550 °C, which means a decrease in porosity. [86] This tells us that we must always have in mind that high porosity and consequently the presence of a higher number of void spaces in the samples structures can result in a decline in mechanical properties which can be critical for implants where high loads are applied. Therefore, it is necessary to adapt the porosity, pore size and thus compressive strength of porous YSZ ceramics depending on its potential applications. Consequently, many researchers have been working with the objective to improve strength while preserving high percentages of porosity. Many approaches have been taking such as reducing pore size or optimizing its shape. However, the reinforcement of the skeleton of porous ceramics by high strength ceramic fibers has shown good results. [87]

Additionally, we can verify that samples F and G present very low percentages of closed porosity. These results are relevant because they show that there is not a large amount of the samples structures that don't not have the ability to flow fluids and that it is not a cause for degradation the performance, the mechanical properties, and the reliability of the samples.

Furthermore, it was possible to obtain samples with densities between 1.95 g/ cm^3 and 2.65 g/ cm^3. If we compare these values with the one's achieved with other biomaterials like alumina (3.98 g/cm3), Y – TZP (6.08 g/cm3) or titanium (4.51 g/cm3) [12] we can obtain less dense samples, however mechanically strong as presented in section 3.5 – Mechanical properties.

3.3 – Crystalline phases

The crystalline phases of the 3 mol% YSZ powder that constituted the samples was investigated by means of X-ray diffraction. The respective diffraction pattern is presented in Figure 4. To get more detailed information, consult the Supporting Information in particular "X- ray diffraction data sheets".

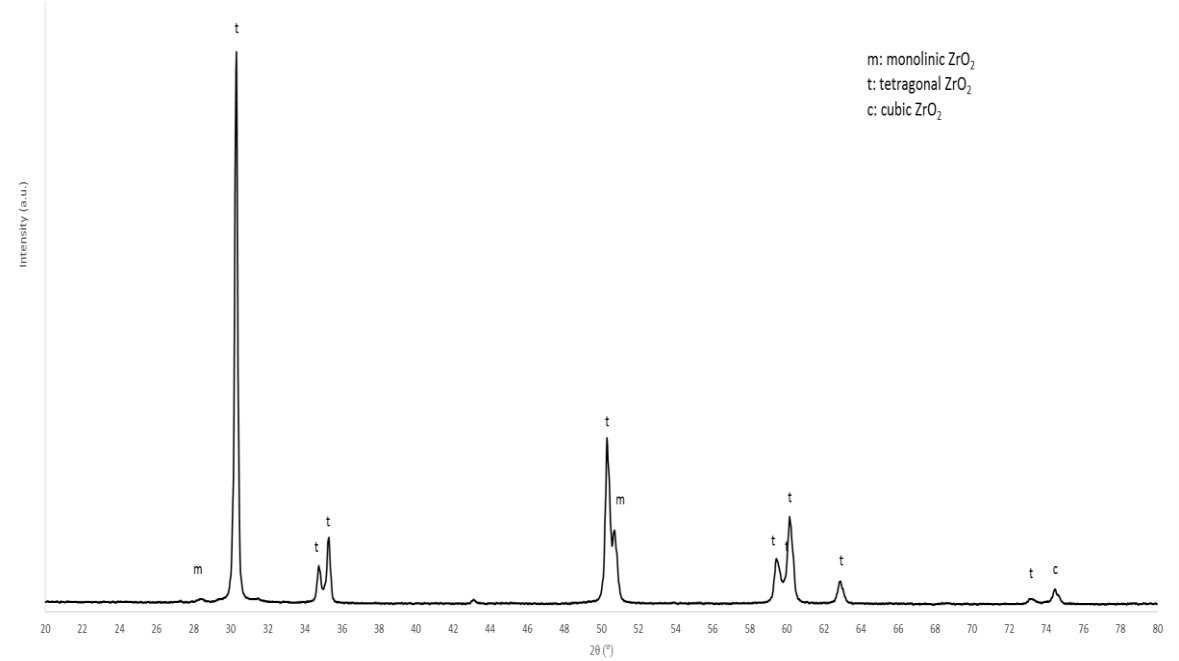

Figure 4 – X-ray diffraction pattern of the 3 mol% YSZ powder.

In this pattern, it is possible to observe that the main phase is tetragonal (t). Also few amount of monoclinic (m) and a significantly cubic (c) phase of ZrO_2 are observed, which are characterized by the diffraction peaks approximately at $2\theta = 28^o$, $2\theta = 50^o$ and $2\theta = 74^o$, respectively.

So we can conclude that during sintering, did not occur a T- M transformation (tetragonal to monoclinic crystal structure) in ZrO_2 or if it happened was in low extent implying that ageing didn't occur. This significantly small presence of the monoclinic phase can be explained by a phenomenon which has already been widely studied called low-temperature degradation (LTD) or hydrothermal degradation. It happens when zirconia is submitted to a humid environment with temperatures between 150 and 400 °C. It is characterized by water's penetration into the structure zirconia inducing the T-M transformation of zirconia.

3.4 – Morphological analysis

Pore size and microstructure play a critical role in osteogenesis of bioceramics *in vitro* and *in vivo*. According to the 1970's Hulbert *et al.* studies [88], the minimum pore size required for an effective migration of cells and nutrients is considered to be approximately 100 µm. Depending on the pores sizes, we can distinguish two types of porosity: macroporosity (pores sizes superior to 50 µm) and microporosity (pores sizes superior to 10 µm). Macroporosity has a strong impact on osteogenic outcomes however the presence of microporosity results in a greater surface area which is believed to contribute to induce a higher protein adsorption into bone. [89] Additionally, small pores favor environments of low oxygen levels and induce osteochondral tissue (composed of bone and cartilage) formation before osteogenesis, while large pores, that are well- vascularized lead to direct osteogenesis (without preceding cartilage formation). [90] In this study, bioceramic samples with pores sizes between approximately 30 µm and 270 µm were obtained. However, as it will be discussed below, these pores resulted mainly from stabilization of air bubbles inside the samples.

In figures 5 to 8, the representative SEM images of the 3YSZ samples are presented. All the SEM images obtained for the samples produced in this work can be seen in the Supporting Information section of this document.

Figure 5 shows the presence of pores inside the samples with the group's code A, B, C, D and E. These pores were created by air bubbles which became confined on the structure of the ceramic samples and which were caused by the fact that during homogenization of the colloidal suspensions the dispersant that was used was responsible for the stabilization of air bubbles, which after lyophilization and sintering developed spherical pores. The presence of these pores created high dispersion of the values of density and porosity, which were detrimental to the mechanical properties. Consequently, it was required to execute rheological studies, to study the viscosity of the suspensions in order to prevent the stabilization of these air bubbles (section 3.6 –Rheological studies).

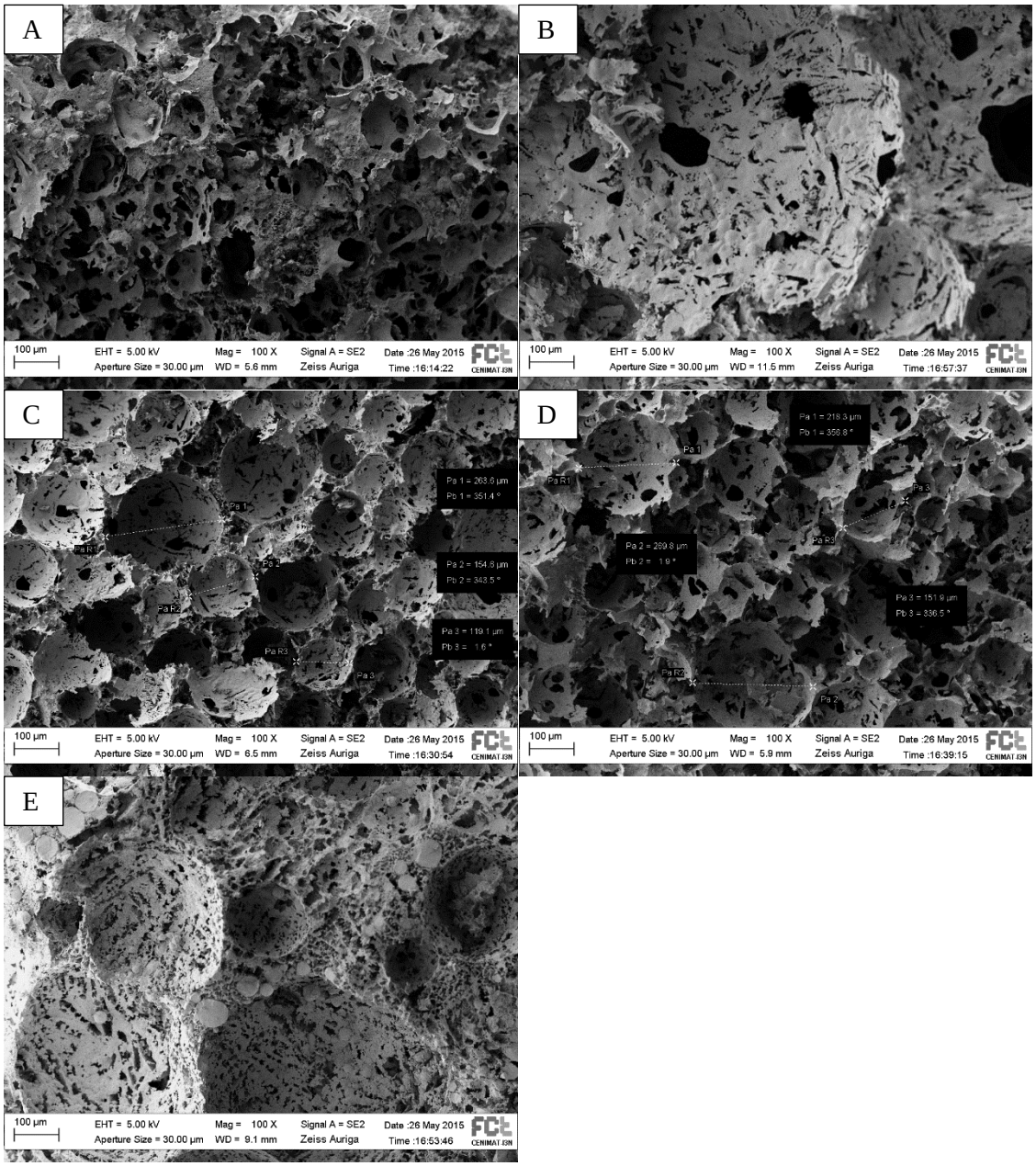

Figure 5 - SEM images of the 3YSZ samples (transverse section) with group's code A, B, C, D and E, highlighting the presence of pores which resulted from the stabilization of air bubbles.

Despite the heterogeneity of the samples, SEM observation at higher magnification (Figure 6) shows that the sintering temperature was adequate to achieve complete densification of the pores' walls.

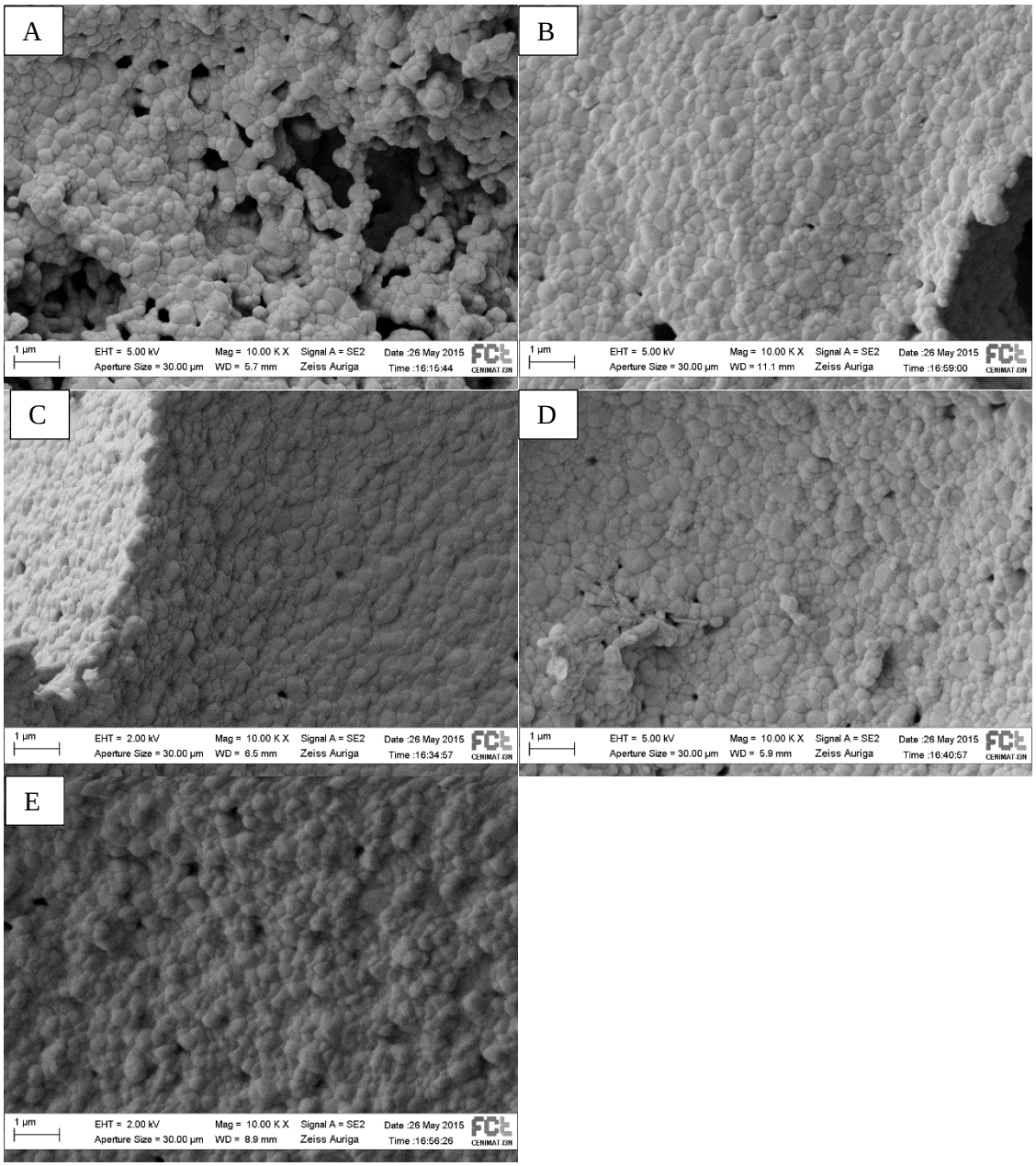

Figure 6 – SEM images of the pores' walls (samples A to E) showing the densification of the structure resultant from the sintering treatment.

3YSZ optimized suspensions (see section 3.6 –Rheological studies) of 40 w_{3YSZ}/w_{Total} % and with higher solid content (50 w_{3YSZ}/w_{Total}%), samples F and G, respectively, were prepared and were morphologically analyzed. SEM images for these samples are presented on Figure 7 and 8.

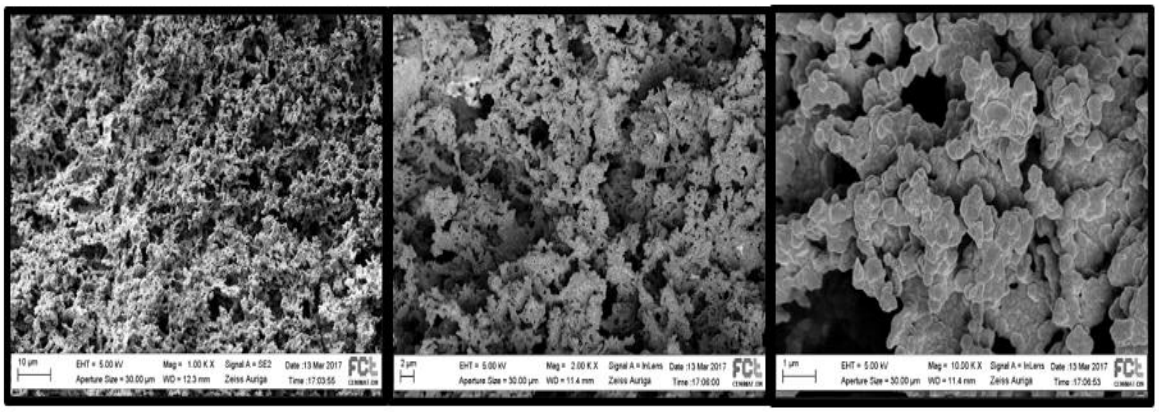

Figure 7 - SEM images of the 3YSZ samples with 40% (w_{3YSZ}/w_{Total}) 3YSZ (sample F).

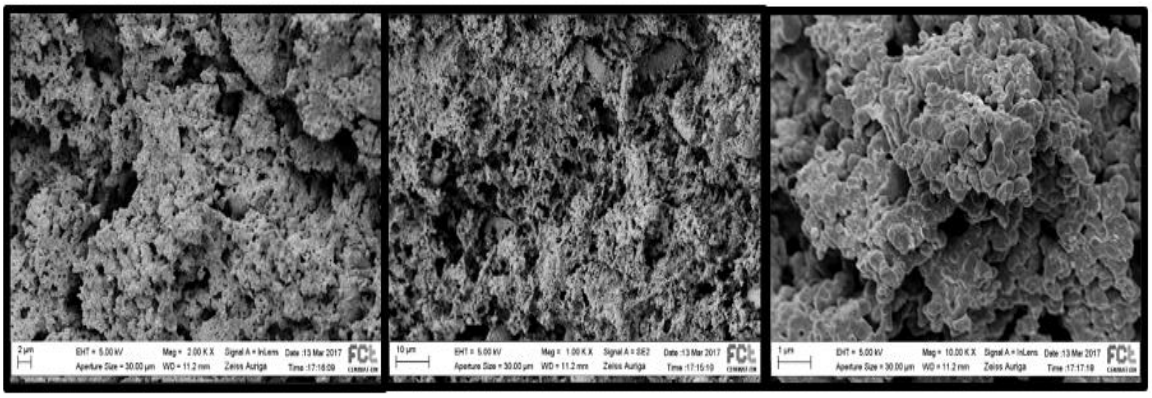

Figure 8 - SEM images of the 3YSZ samples with 50% (w_{3YSZ}/w_{Total}) 3YSZ (sample G).

As can be observed into the two images above, we can sustain that the open porosity is inferior in the samples with 50% 3YSZ. Even though the difference of porosities is not significant, we can confirm the porosity measurements documented in section 3.2 – Density and Porosity (a difference of approximately 12%). Higher magnification images of figure 7 and 8 also show the densification of the pores' walls resultant from the sintering treatment.

3.5 – Mechanical properties

A typical stress – strain curve is exemplified in Figure 9 which is characterized by presenting three very well defined regimes: a region of linear elasticity (low ε), a stress plateau and a region of densification (high ε).

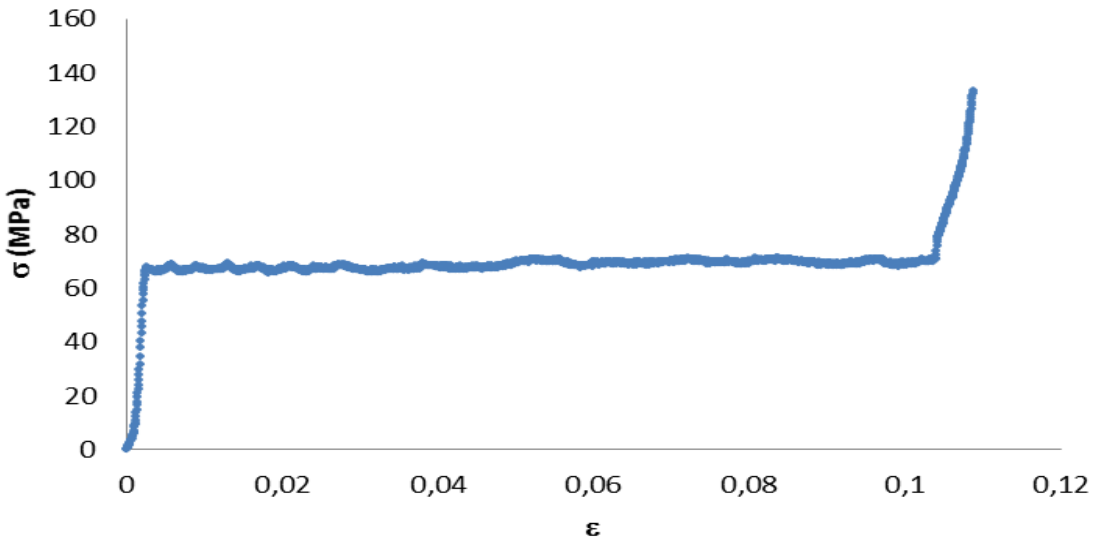

Figure 9 – Stress – strain curve of sample G4. All the samples showed similar mechanical behavior presenting the 3 regions in the stress-strain curve.

In the elastic regime, stress increases linearly with strain until the upper yield point which can be expressed by Equation 1

$$\sigma = E\,\varepsilon \qquad \textbf{Equation 1}$$

where E is the Young's modulus (or elastic modulus) and it can be determined by calculating the initial slope of the stress-strain response of the ceramic porous foams. The stress plateau is described by an extensive collapse plateau in which the stresses do not fluctuate a lot, followed by a region of increasing stress that corresponds to the densification which matches to the compaction of the pores of the foams. According to Michael F. Ashby [91], the extent of each regime depends on the relative density of the foam $\left(\frac{\rho}{\rho_s}\right)$, where ρ is the bulk density of the foam and ρ_s, the density of the solid of which the foam is made. For an open-cell foam, the linear elastic properties can be studied by equation 2

$$\frac{E}{E_s} = \left(\frac{\rho}{\rho_s}\right)^2 \qquad \textbf{Equation 2}$$

where E is the Young's modulus, E_s is the elastic modulus of the material of which the foam was made (which for dense tetragonal zirconia is about 200 GPa [92]) and C is a constant (usually C = 1.)

Also according to Ashby's model, the collapse stress of an open-cell foam can be expressed by equation 3

$$\frac{\sigma_{pl}^*}{\sigma_y} = C_1 \left(\frac{\rho}{\rho_s}\right)^{3/2} \qquad \textbf{Equation 3}$$

where σ_{pl}^* is the collapse stress, σ_y is the bending strength and C_1 is a constant ($C_1 \cong 0.2$ [94]). Typically, σ_y for 3YSZ is between 900 - 1200 MPa. [93].

The values of Young's modulus and collapse stresses of the sintered samples are presented in Table 5.

Table 5 - Variation of Young's modulus and collapse stresses.

Samples' s Group Code	E (GPa)	σ_{pl}^{*} (MPa)
A	1.80 ± 0.80	43.00 ± 3.00
B	2.90 ± 1.80	42.00 ± 1.00
C	3.10 ± 0.90	41.00 ± 15.00
D	3.30 ± 1.60	32.00 ± 12.00
E	5.30 ± 2.40	37.00 ± 11.00
F	27.40 ± 8.20	66.90 ± 4.30
G	28.60 ± 4.40	70.10 ± 3.10

By evaluating the results of the samples with the group's code A, B, C, D and E, we can stand that the Young modulus and the collapse stresses are relatively low. This is caused by the presence of pores which are developed by the air bubbles already identified using SEM (see section 3.4 - Morphological analysis). During the colloidal suspensions homogenization, AOT stabilized air bubbles which after the process of lyophilization and sintering formed spherical pores which consequently allow the presence of a high number of void spaces which result in a decline in the mechanical properties. Consequently, rheological studies were performed (section 3.6 – Rheological studies), to evaluate the viscosity of the colloidal suspensions in order to prevent the stabilization of the air bubbles. The outcome was the manufacture of the samples with codes F and G. Consequently, it was possible to obtain porous foams with elastic modulus between 19.20 GPa and 35.60 GPa and collapse stress between 62.60 MPa and 73.10 MPa.

The mechanical properties of the foams (Young modulus and collapse stress) where compared to those obtained by Ashby's model for open-cell foams, according to equations 2 and 3. Relative density in Ashby's model, $\rho_r = \frac{\rho}{\rho_s}$ is related to the total porosity of the foams by $\phi = 1 - \rho_r$. For open-cell foams ϕ is in fact the open porosity (since no closed pores are considered in this case). In our case we have both open and closed porosity. However, as it can be seen from the results of table 4, for the foams F and G the closed porosity is very small when compared to the open porosity and for that reason we have considered $\phi \approx P_o$ (open porosity determined by the Arquimedes' method).

The information presented in Table 6 allows us to assess in which degree Youngs' Modulus of our foams agree with those predicted by Ashby's model.

Table 6 – Comparison between the Young Modulus obtained versus calculated by Ashby model.

% 3YSZ (w_{3YSZ}/w_{Total}) on the sample	P_o	$\left(\frac{\rho}{\rho_s}\right)^2$	E (GPa) experimental	E (GPa) according to eq. (2)
40	0.65 (65%)	0.1225	27.40	24.50
50	0.53 (53%)	0.2209	28.69	44.18

These results show us that for high levels of open porosity there is a good agreement between the obtained elastic modulus and the theoretical one's calculated by the model of Ashby. However,

the concordance is lost for lower porosities, which is expected since Young Modulus determined by equation 2 are closer to the experimental values for $\phi > 70\%$ [91].

In table 7, we compare the obtained values of σ_{pl}^{*} which correspond to the stresses in the region of plateau and the theoretical values of $\sigma_{pl\,min}^{*}$ and $\sigma_{pl\,max}^{*}$ using $\sigma_{y\,min}$ = 900 MPa and $\sigma_{y\,max}$ = 1200 MPa, respectively, and following the model of Ashby.

Table 7 – Comparison between the collapse stresses obtained versus calculated by Ashby model.

% 3YSZ (w_{3YSZ}/w_{Total}) on the sample	**P_o**	**σ_{pl}^{*} (MPa)**	**$\left(\frac{\rho}{\rho_s}\right)^{\frac{3}{2}}$**	**$\sigma_{pl\,min}^{*}$ (MPa) according to eq. (3)**	**$\sigma_{pl\,max}^{*}$ (MPa) according to eq. (3)**
40	0.65 (65%)	66.90	0.2071	37.27	49.70
50	0.53 (53%)	70.10	0.3222	58.00	77.33

With these results, we can see that for the lowest levels of porosity, there is a good agreement between the obtained collapse stresses and the theoretical one's calculated by the model of Ashby. Being the collapse stress, a property related with the compaction of the structure, and therefore, obtained outside the elastic regime, it is not particularly odd that unlike Young's modulus, the agreement between the obtained collapse stresses and the theoretical one's is superior to foams with lower porosity.

For bioceramic implants, particularly as load bearing parts, the elastic modulus and the collapse stress must be as much as possible similar to those of natural bone. In table 8, we compare the obtained values of Young modulus and collapse stresses with the one's which are proper of the cortical bone (also known as compact bone which forms the extremely hard exterior of long bone's) and cancellous bone (or trabecular bone which is highly vascular and frequently contains red bone marrow).

Table 8 – Evaluation of the mechanical properties of the porous samples vs the human bone [95].

Mechanical property	**Cortical bone**	**Cancellous bone**	**40% 3YSZ (w_{3YSZ}/w_{Total})**	**50% 3YSZ (w_{3YSZ}/w_{Total})**
Young Modulus (GPa)	7-30	0.5 – 0.05	27.40 ± 8.20	28.60 ± 4.40
Compressive Strenght (MPa)	100-230	2-12	66.90 ± 4.30	70.10 ± 3.10

The values of density and elastic modulus of the foams containing 40% 3YSZ are about 2.03 g/ cm^3 and 27.40 GPa, respectively. Yet, as the 3YSZ content increased, their values increased also due to a decrease of porosity. In the samples which contained 50% 3YSZ, the values of density and elastic modulus are about 2.62 g/ cm^3 and 28.60 GPa, respectively. From these results, we can conclude that the values of elastic modulus of the porous foams are almost the same as the human cortical bone, which is particularly interesting for orthopedic and dentistry applications.

When we compare our results with the one's obtained with freeze-casting [85], it is possible to sustain that by using freeze-drying we obtained high-porosity zirconia ceramics with higher compressive strengths. Additionally, we also obtained porous yttria-stabilized zirconia ceramics

with better mechanical properties than the one's achieved by Zuo *et al.* that also used aqueous ceramic slurries of yttria-stabilized zirconia and PVA as a binder. [96]

As referred before, the sintering temperature of the porous YSZ ceramics influences significantly the porosity, pore size, linear shrinkage, and consequently the compressive strength. Therefore, it is possible to increase sintering temperature to improve the control of the densification and thus the compressive strength of porous YSZ ceramics for potential biomedical applications.

3.6 – Rheological studies

As previously referred and as shown on section 3.4 - Morphological analysis, during the process of homogenization of the colloidal slurries, the dispersant used stabilized air bubbles which after lyophilization and sintering resulted in the formation of spherical pores which gave rise to uncontrolled porosity that consequently made us achieve inconsistent results.

Therefore, and in order to reduce the suspensions viscosity, 40% and 50 % 3YSZ were manufactured, the percentage of AOT was reduced to 2.5% (w_{AOT}/w_{3YSZ}) and TMAH was added. TMAH is a strong base and has the ability to change the surface charge of the nanoparticles which enables achieving adequate distance between them and consequently reducing agglomeration. Figure 10 presents the effect of TMAH on the viscosity of the aqueous ceramic slurries of yttria-stabilized zirconia.

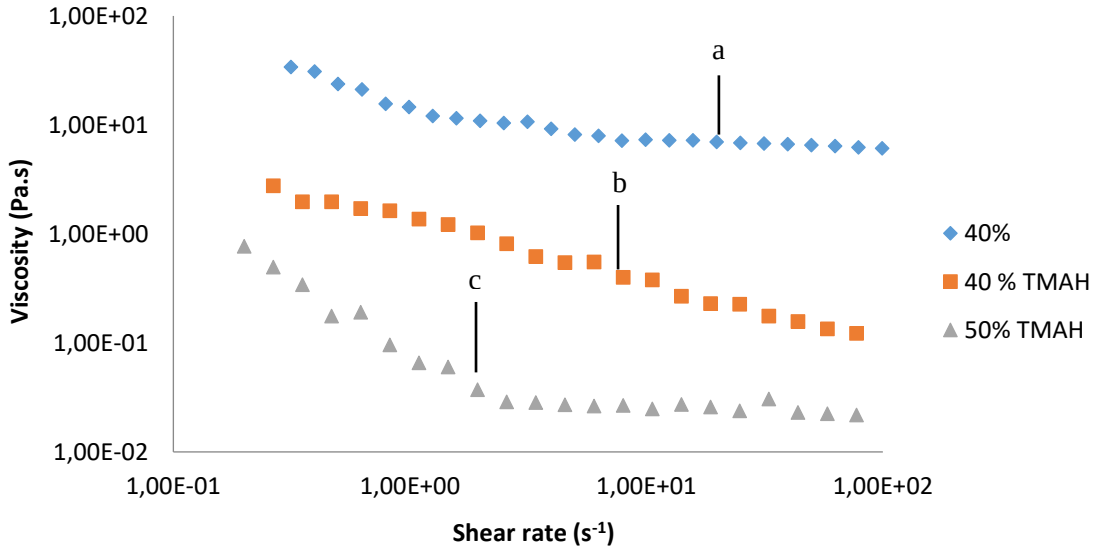

Figure 10 – Viscosity curves for the nanosuspensions: (a) 40% YSZ without using TMAH, (b) 40% YSZ using TMAH and (c) 50% YSZ after multiultrasound treatments.

The 50 % 3YSZ suspension with TMAH was subject to a multiultrasound treatment because it has been shown that by using ultrasounds is possible to destroy agglomerates that can be form. Multiultrasound involves applying ultrasound energy to the suspensions at several different points in the concentration process until the required solids loaded is completed. [97]. In our case, it involved a 3-stage multiultrasound treatment (2 min at 1/3 of the final concentration, 2 min at 2/3 of the final concentration and 2 min at the final concentration). The 40 % 3YSZ suspension with TMAH didn't had this treatment because according to Innovnano for this percentage, the suspension is already stable, which indeed we verified. However, as it can be seen from figure 10 the viscosity of the 40% suspension without TMAH is too high, which is responsible for the

heterogeneous structures obtained. Therefore, TMAH was only added with the intent to decrease the viscosity of the suspension, which is shown in figure 10.

It is likely to assume that with multiultrasound treatments, it is possible to obtain low viscosity suspensions even for a higher content of 3YSZ, which means that in a future work we must go in this direction, i.e., increasing even more the percentage of the 3YSZ powder in the ceramic slurries.

4 – Conclusions and Future Perspectives

This dissertation focused on the production of quality 3 mol % yttria partially stabilized tetragonal zirconia porous foams, applying a freeze drying process followed by sintering, and using as a starting material a 3YSZ nanosized crystalline powder, provided by Innovnano– Materiais Avançados S.A. Freeze drying was chosen since it has been widely explored and used in the production of bioceramics allowing the production of porous foams with different morphologies and rates of porosities. Besides, this method is low cost, simple and can be easily upgraded to actual companies processing methods with small resources investments.

Yet, inconsistencies were found in our results as shown on Chapter 3. These results were the consequence of the presence of spherical pores created by air bubbles confined in the porous foams' structures. These pores were produced by the fact that during the homogenization of the colloidal suspensions, the dispersant used (AOT) was responsible for stabilizing air bubbles which after lyophilization and sintering produced spherical pores. Therefore, it was required to do some further research on our method of manufacturing the ceramic suspensions. Therefore, the viscosity of the suspensions was reduced in order to allow a better treatment/ stabilization and to avoid the presence of air bubbles while freezing and before lyophilization. In addition, the rheological studies permitted to stand that by using multiultrasound treatments, it was possible to decrease the value of suspension's viscosities for higher contents of 3YSZ. And so, in a future work, multiultrasound treatments must be optimized in order to increase even more the percentage of nanopowder in the ceramic slurries.

Using the Archimedes method, it was possible to measure the open/closed porosities and densities of the produced foams. Foams with open porosities between 52.10% and 67.60% and densities between 1.95 g/ cm^3 and 2.65 g/ cm^3 were produced. These results lie above what is common to achieve since it is challenging to produce highly porous foams of yttria-stabilized zirconia with porosity percentages higher than 50%. Additionally, it was possible to obtain better results that the ones previously achieved using other sorts of ceramic manufacturing processes (e.g. gelcasting). Also, by using a low sintering temperature, it was possible to obtain slightly dense samples, however mechanically robust.

Using X-ray diffraction, it was observed that the main crystallographic phase present in the porous samples is tetragonal. Consequently, it is possible to conclude that during sintering a T-M transformation in zirconia did not occur from tetragonal to monoclinic crystal structure implying that ageing did not occur, which means that did not take place a loss in density and a reduction in strength/ toughness during sintering.

By means of SEM, a morphological analysis of the 3YSZ samples was obtained. Bioceramic samples with pores sizes between approximately 30µm and 270 µm were produced. These relatively large pores are advantageous for promoting bone ingrowth.

Compression tests on the porous samples revealed elastic modulus between 19.20 GPa and 35.60 GPa and collapse stress between 62.60 MPa and 73.10 MPa. Additionally, we concluded that the values of elastic modulus are similar to the ones of the human cortical bone and much higher than the trabecular bone. These results are quite motivating and should be improved, e.g. by increasing the solids content in the ceramic slurries.

In the future, an increase of the sintering temperature should also be considered. Despite the good densification of the pores' walls achieved in this work, further improvements could lead to higher values of the compressive strength of porous YSZ ceramics beneficial for potential biomedical applications.

Additionally, and with the intent to obtain even better results on mechanical properties, it would be proper to study and optimize the 3YSZ slurries including the percentages of binder (PVA) and surfactant (AOT), being appropriate to optimize the sintering steps and sintering temperatures used during the manufacturing process (perform densification studies) since the ones used in this dissertation were recommended by Innovnano. However in their control and quality studies, the samples are only made by 3YSZ.

In addition, it is suggested to carry out this work by using another method to manufacture 3YSZ porous foams, such as 3D printing. Therefore, it will be possible to compare the results obtained with the one's achieved by using the lyophilization process in order to verify that if exits a decrease in density, an increase in porosity and an improvement on the mechanical properties.

Although being reported in the literature the biocompatibility of 3YSZ powders, it is highly recommendable and mandatory for biomedical applications to perform cytotoxicity studies to confirm this. *In vitro* and *in vivo* studies to access the influence of water in the stability (to evaluate possible ageing processes) should also be performed.

5 – References

[1] Biomaterials - Latest research and news, Nature. Available at: http://www.nature.com/subjects/biomaterials. [Accessed 17 Aug. 2016]

[2] Hench L., "Bioceramics", *J. Am. Ceram. Soc.*, vol. 81, pp. 1705–1728, 1998.

[3] Abraham M.A., "A Brief Historical Perspective on Dental Implants, Their Surface Coatings and Treatments", *Open Dent J*., vol. 8, pp. 50–55, 2014.

[4] Albrektsson T, Brånemark PI, Hansson HA, Lindström J., "Osseointegrated titanium implants. Requirements for ensuring a long-lasting, direct bone-to-implant anchorage in man, *Acta Orthop Scand.,* vol.52, pp. 155-170, 1981.

[5] Adya N., Alam M., Ravindranath T., Mubeen A., Saluja B., "Corrosion in titanium dental implants: literature review", *J Indian Prosthodont Soc*, vol.3, pp. 126-131, 2005.

[6] Souza, Júlio C. M., Henriques, Mariana; Teughels, Wim; Ponthiaux, Pierre; Celis, J.P.; Luís A. Rocha, "Wear and corrosion interactions on titanium in oral environment: literature review", Journal of Bio- and Tribo-Corrosion, pp. 1-13, 2015.

[7] Chaturvedi T.P, "Allergy related to dental implant and its clinical significance", *Clin Cosmet Investig Dent*., vol. 5, pp. 57–61, 2013.

[8] Frisken K.W., Dandie G.W., Lugowski S., Jordan G., "A study of titanium release into body organs following the insertion of single threaded screw implants into the mandibles of sheep", *Aust Dent J*., vol. 47, pp. 214-217, 2012.

[9] Smith D.C., Lugowski S., McHugh A., Deporter D., Watson P.A., Chipman M., "Systemic metal ion levels in dental implant patients", *Int J Oral Maxillofac Implants*, vol. 12, pp. 828-34, 1997.

[10] Lugowski S.J., Smith D.C., McHugh A.D., Van Loon J.C., "Release of metal ions from dental implant materials in vivo: determination of Al, Co, Cr, Mo, Ni, V, and Ti in organ tissue", *J Biomed Mater Res.*, vol. 25, pp.1443-58, 1991.

[11] De Aza A., Chevalier J., and Fantozzi G., "Crack growth resistance of alumina, zirconia and zirconia toughened alumina ceramics for joint prostheses," *Biomaterials*, vol. 23, pp. 937–945, 2002.

[12] Rashid H., "The effect of surface roughness on ceramics used in dentistry: A review of literature", *Eur J Dent.*, vol.8, pp. 571–579, 2014.

[13] Wenz H.J., Bartsch J., Wolfart S., Kern M., "Osseointegration and clinical success of zirconia dental implants: a systematic review", *Int J Prosthodont*, vol.21, , pp. 27-36, 2008.

[14] Schulte W., "The intra-osseous Al2O3 (Frialit) Tuebingen implant. Developmental status after eight years (I-III)", *Quintessence Int*, vol. 15, pp. 1–39, 1984.

[15] Maccauro G., Rossi I.P, Raffaelli L. and Manicone P.F., "Alumina and Zirconia Ceramic for Orthopaedic and Dental Devices", *Biomaterials Applications for Nanomedicine*, 2011.

[16] Berge T.I., Grønningsaeter A.G., "Survival of single crystal sapphire implants supporting mandibular overdentures", *Clin Oral Implants Res.*, vol. 11, pp. 154-62, 2000.

[17] Pigot J. L., Dubruille J. H., Dubruille M. T., Mercier J. P., Cohen P., "Les implants en céramique au secours de la prothèse totale inférieure", *Revue de stomatologie et de chirurgie maxillo-faciale,* vol. 98, pp. 10-13 ,1997.

[18] Thoma D.D., Benic G.I., Munõz F, *et al.,* "Histological nalysis of loaded zirconia and titanium dental implants: an experimental study in the dog mandible ", *J clin Periodontol,* vol. 42, pp. 967-975, 2015.

[19] Deepprich R., Naujoks C. Ommerborn M., et al. "Current indings regarding zirconia implants ", *Clin Implant Den Relat Res.,* vol.16, pp.124-137, 2014.

[20] Sennerby L., Dasmah A., Larsson B, *et al.* "Bone tissue responses to surface-modified zirconia implants: a histomorphometric and removal torque study in the rabbit ", *Clin Implant Dent Res,* vol.7, pp. 13-20, 2005.

[21] Wennerberg A., Albrektsson T., Jimbo R., "Implant surfaces and their biological and clinical impact ", *New York,* pp.93-136, 2014.

[22] Gahlert M., Wieland M., *et al.* "A comparison study of the osseointegration of zirconia and titanium dental implants. A biomechanical evaluation in the maxila of pigs ", *Clin Implant Relat Res,* vol.12, pp. 297-305, 2010.

[23] Gahlert M., Roehling S., Sprecher C.M., *et al.,* "In vivo performance of zirconia and titanium implants: a histomorphometric study in mini pig maxillae ", *Clin Oral Implants Res.,* vol. 23, pp.281-286, 2012.

[24] Nkamgeu E.M., Adnet J.J., Bernanrd J., *et al.*, "In vitro effects of zirconia and alumina particles on human blood monocyte-derived macrophages: X-ray microanalysis and flow cytometrix studies, *J Biomed Mater Res.,* vol.52, pp. 587-798, 2000.

[25] Dion I., Rouais F., Baquey C., *et al.* "Physico-chemistry and cytotoxicity of ceramics", *J Mater Sci Mater Med,* vol.8, pp.325-332, 1997.

[26] Rimondini L., Cerroni L. Carrassi A., *et al.* "Bacterial colonization of zircónia ceramic surfaces: an in vitro and in vivo study, *Int J Oral Maxillofac Implants,* vol. 52, pp.587-594, 2000.

[27] Roehling S., Woelfler H., Hicklin S. *et al.*, "A restrospective clinical study with regard to survival and success rates of zirconia implnats up to and after 7 years of loading", *Clin Impnat Dent Relat Resp.,* vol.18, pp.545-558, 2016.

[28] Jung R.E, Grohmann P., Sailer I, *et al.,* "Evaluation of a one-piece ceramic implant used for single-tooth replacement and three-unit fixed partial dentures: a prospective cohort clinical trial, *Clin Oral Implants Res.,* vol.27, pp.751-761, 2016.

[29] Siddiqi A., Kiesser J.A., De Silva R.K., *et al.* "Soft and hard tissue response to zirconia versus titanium one-piece implants placed in alveolar and palatal sites: a randomized control trial, *Clin Implant Dental Relat Res.*, vol.17, pp.483-496, 2015.

[30] Kohal R.J., Schwindling F.S., Bachle M., *et al.*, "Peri-implant bone response to retrieved human zirconia oral implants after a 4-year loading period: a histologic and histomorphometric evaluation of 22 cases, *J Biomed Mater Res B appl Biomater.*, pp.1-10, 2015.

[31] Kniha K., Gahlert M., Hicklin S., *et al.*, "Evaluation of hard and soft tissue dimensions around zirconium oxide implant-supported crowns: a 1-Year retrospective study, *J Periodontol*, vol.87, pp.511-518, 2016.

[32] Rutkanas V., Bukelskiene V., Sabaliauskas V., *et al.*, "Assessment of human gingival fibroblast interaction with dental implant abutment materials ", *J Mater Sci Mater Med.*, vol.26, pp.5481-5488, 2015.

[33] Okabe E., Ishihara Y., Kikuchi T., *et al.*, "Adhesion properties of human oral epithelial-derived cells to zirconia", *Clin Implant Dent Relat Res.*, pp. 1-11, 2015.

[34] Abrahamsson I., BErglundh T., Glantz PO, *et al.*, The mucosal attachment at different abutments. An experimental study in dogs", *J Clin Periodontol*, vol.25, pp.721-727, 1998.

[35] Zembic A., Sailer I., Jung R. *et al.*" Randomized-controlled clinical trial of customized zirconia and titanium implant abutments for single-tooth implants in canine and posterior regions: 3-year results", *Clin Oral Implants Res.*, vol.20, pp.802-808, 2009.

[36] Zembic A., Bosch A., Jung R., *et al." Five*-year results of a randomized controlled clinical trial comparing zirconia and titanium abutments supporting single-implant crowns in canine and posterior regions", *Clin Oral Implants Res.*, vol.24, pp.384-390, 2013.

[37] Thoma D.S., Ioannidis A., Cathomen E., *et al.*, "Discoloration of the peri-implant mucosa caused by zirconia and titanium implants, *Int J Periodontics Restorative Dent.*, vol.36, pp.39-45, 2016.

[38] Cooper L.F., Stanford C., Feine J., *et al.*, "Prospective assessment of CAM/CAM zirconia abutment and lithium disilicate crown restorations: 2,4 year results", *J Prosthet Dent*, vol.28, pp.144-156, 2016.

[39] Hiroaki Y., Kunihito K., Masaru M., "The chemistry of ceramics", *Wiley*, p. 248, 1996.

[40] Saridag S., Tak O., and Alniacik G., "Basic properties and types of zirconia: An overview," *World J. Stomatol*, vol. 2, pp. 40–47, 2013.

[41] Kohal R.J., Att W., Bächle M., Butz F., "Ceramic abutments and ceramic oral implants. An update", *Periodontol*, vol. 47, pp. 224-43, 2008.

[42] Volpato C.A.M., Altoé G.L.G. ´, Fredel M.C. and Bondioli F., "Application of Zirconia in Dentistry: Biological, Mechanical and Optical Considerations", *Advances in Ceramics - Electric and Magnetic Ceramics, Bioceramics, Ceramics and Environment*, 2011.

[43] Chevalier, J., *et al.,"*Critical effect of cubic phase on aging in 3 mol% yttria-stabilized zirconia ceramics for hip replacement prosthesis, *Biomaterials*, Vol. 25, pp. 5539–5545, 2004.

[44] Kurtz S. M., Kocagöz S., Arnholt C., Huet R., Ueno M., and Walter W. L., "Advances in zirconia toughened alumina biomaterials for total joint replacement.," *J. Mech. Behav. Biomed. Mater.*, vol. 31, pp. 107–16, 2014.

[45] Chevalier, J., *et al.* "The Tetragonal-Monoclinic Transformation in Zirconia: Lessons Learned and Future Trends," *J. Am. Ceram. Soc.*, vol. 92, pp. 1901–1920, 2009.

[46] Denry I., Kelly J.R..,"State of the art of zirconia for dental applications", *Dent Mater*. vol. 24, pp. 299–307, 2008.

[47] and Zarone F., Russo S., Sorrentino R., "From porcelain-fused-to-metal to zirconia: clinical experimental considerations", *Dent Mater.*, vol. 27, pp.83–96, 2011.

[48] Tekeli, S. and Demir, U. "Colloidal processing, sintering and static grain growth behaviour of alumina-doped cubic zirconia", *Ceramics International,* vol.31, pp .973–980, 2005.

[49] Yen-Wei C., Moussi J., Drury J.L., and Wataha J.C., "Zirconia in biomedical applications", *Expert Review Of Medical Devices* Vol. 13, pp. 101-102, 2016.

[50] Palmeroa P, *et al.*, "Towards long lasting zirconia-based composites for dental implants. Part I: Innovative synthesis, microstructural characterization and in vitro stability", *Biomaterials*, vol. 50, pp. 38–46, 2015.

[51] Fischer J., Stawarczyk B., "Compatibility of machined Ce-TZP/Al2O3 nanocomposite and a veneering ceramic", vol.23, pp. 1500–1505, 2007.

[52] Gahlert M., Burtscher D., Pfundstein G., *et al.* "Dental zirconia implants up to three years in function: a retrospective clinical study and evaluation of prosthetic restorations and failures", *Int J Oral Maxillofac Implants,* vol. 28, pp.896-904, 2013.

[53] Liang H., Chang-An W., Yong H., "Porous yttria-stabilized zirconia ceramics with ultra-low thermal conductivity", *J Mater Sci*, vol. 45, pp. 3242–3246, 2010.

[54] European Comission," COMMISSION RECOMMENDATION of 18 October 2011 on the definition of nanomaterial", *Official Journal of the European Union,* 2011.

[55] Heitjans P. and Indris S*.,* "Diffusion and ionic conduction in nanocrystalline ceramics*", Journal of Physics: Condensed Matter,* vol.15, 2003.

[56] Mayo M.J., Hague D.C., Chen D.-J., "Processing nanocrystalline ceramics for applications in superplasticity", *Materials Science and Engineering: A,* vol. 166, pp. 145-159, July 1993.

[57] Holister P., Román C., Harper T., "Nanocrystalline Materials – Technology White Papers, C*ientifica*, 2003.

[58] Santos R., "Transparent Nanocrystalline Glass Ceramics", Available at: https://fenix.tecnico.ulisboa.pt/downloadFile/395137847235 [Accessed 17 Aug. 2016].

[59] Binner J., "Processing of bulk nanostructured ceramics", *Journal of the European Ceramic Society*, vol. 28, pp. 1329–1339, 2008.

[60] Emulsion Detonation Synthesis (EDS): Our patented manufacturing technology, Innovnano. Available at: http://www.innovnano-materials.com/our-technology/ [Accessed 17 Aug. 2016].

[61] Raghupathy B., Binner J., “Spray freeze drying of YSZ nanopowder”, *Journal of Nanoparticle Research,* vol.14, 2012.

[62] Huang T.S., Rahaman M.N., Doiphode N.D., *et al.* “Porous and strong bioactive glass Scaffolds fabricated by freeze extrusion technique” *Mater Sci Eng,* vol.31, pp.1482–1489, 2011.

[63] Doiphode N.D., Huang T., Leu M.C., Rahaman M.N., “Day DE. Freeze extrusion fabrication of 13-93 bioactive glass scaffolds for bone repair” *J Mater Sci Mater Med,* vol. 22, pp. 515 -523, 2011.

[64] Deville S., “Freeze-casting of porous ceramics: a review of current achievements and issues” *Adv Eng Mater*., vol.10, pp.155–169, 2008.

[65] Lebreton K., Rodrıguez-Parra J.M., Moreno R., Nieto M.I., “Effect of additives on porosity of alumina materials obtained by freeze casting” *Adv Appl Ceram.*, vol. 114, pp. 296–302, 2015.

[66] Deville S., Saiz E., Tomsia A.P., “Ice-templated porous alumina structures” *Acta Mater.* Vol. 55, pp. 1965–1974, 2005.

[67] Tallon C., Moreno R., Nieto I.M., “Shaping of porous alumina bodies by freeze casting”, *Adv Appl Ceram*, vol.108, pp. 307–313, 2009.

[68] Mayo, M.J., Hague, D.C., Chen, D.J., Processing nanocrystalline ceramics for applications in superplasticity, *Materials Science and Engineering: A*, Vol. 166, pp. 145-159, 1993.

[69] Rittner, M.N. and Abraham, T. ‘‘Economics: Nanostructured Materials: An Overview and Commercial Analysis,’’ *JOM*, vol. 50, pp. 1160–1196, 1998.

[70] Franks G.V., Lange F.F., “Plastic-to-brittle transition of saturated, alumina powder compacts”, *J Am Ceram Soc,pp,* vol. 79, pp.3161– 3168, 1996.

[71] Hunter R.J., Foundations of Colloid Science, 2nd edn. Oxford; New York: Oxford University Press, 2001.

[72] Franks G.V., Colloids and fine particles. In: Rhodes M, eds. Introduction to Particle Technology. *Chichester, UK: John Wiley & Sons,* Ltd, pp.117–152, 2008

[73] Rahaman, M.N., “Ceramic processing and sintering (2nd ed.)”. *New York: Dekker,* pp. 30-32, 343, 2003.

[74] Rahaman, M.N., “Ceramic processing and sintering (2nd ed.)”. *New York: Dekker,* 2003.

[75] Santacruz I., Binner J., Nieto M. I., and Moreno R., “Dispersion and Rheology of Aqueous Suspensions of Nanosized $BaTiO_3$, *J. Am. Ceram. Soc.*, 2007.

[76] Boschmi F., Rulmont A., Cloots R. and Moreno R., “Colloidal Stability of Aqueous Suspensions of Barium Zirconate”, J. Eur. Ceram. Soc., vol.25, pp. 3195-3201, 2015.

[77] Boccaccini , A.R., Reinhard C., “Isotropic shrinkage of platelet containing glass powder compacts during isothermal sintering”, *International Journal of Inorganic Materials*, pp. 101–106, 2001.

[78] Takahasi Y., Tabata Y., “Effect of the fiber diameter and porosity of non-woven PET fabrics on the osteogenic differentiation of mesenchymal stem cells”, *J Biomater Sci Polym* , vol.15, pp. 41-57, 2004.

[79] Souza S., Visco S., Jonghe L., “Thin-film solid oxide fuel cell with high performance at low temperature”, *Solid State Ionics*, vol. 98 pp. 57–61, 1997

[80] López-Gándara C., Ramos F.M and Cirera A., “YSZ-Based Oxygen Sensors and the Use of Nanomaterials: A Review from Classical Models to Current Trends”, *Journal of Sensors*, vol. 2009, 2009.

[81] Clarkea David, Phillpotb Simon, “Thermal barrier coating materials”, *Materials Today*, vol. 8, pp. 22–29, 2005.

[82] Kim H., Rosa C., Boaro M., Vohs J., and Gorte Raymond J., “Fabrication of Highly Porous Yttria-Stabilized Zirconia by Acid Leaching Nickel from a Nickel-Yttria-Stabilized Zirconia Cermet”, *Journal American Ceramics Society*, vol.85, pp. 1473–1476, 2002.

[83] Yunfeng G., Xingqin L., Guangyao M., Dingkun P., “Porous YSZ ceramics by water-based gelcasting”, *Ceramics International,* vol. 25, pp. 705–709, 1999.

[84] LiangFa H., Chang-An W., Yong H., “Porous yttria-stabilized zirconia ceramics with ultra-low thermal conductivity”, *J Mater Sci*, vol.45, pp.3242–3246, 2010.

[85] Changqing H., Xinghong Z., Jiecai H., Jiancong D. and Wenbo H., “Ultra-high-porosity zirconia ceramics fabricated by novel”, *Scripta Materialia*, vol.60, pp.563–566, 2009

[86] LiangFa H., Chang-An W., “Effect of sintering temperature on compressive strength of porous yttria-stabilized zirconia ceramics”, *Ceramics International,* Vol. 36, pp. 1697–1701, 2010.

[87] Ying L.,Chang-An W., Shengnian T., “Porous YSZ Ceramics Reinforced by Different Kinds of Fibers”, *International Journal of Applied Ceramic Technology*, Vol. 11, pp. 824–831, 2014.

[88] Hulbert S. F., Young F. A., Mathews R. S., Klawitter J. J., Talbert C. D., Stelling F. H., “Potential of ceramic materials as permanently implantable skeletal prostheses”, Journal of Biomedical Materials Research Part A”, vol. 4, pp. 433- 456.

[89] Yuan H., Kurashina K., de Bruijn J.D., Li Y-, de Groot K., Zhang X., “A preliminary study on osteoinduction of two kinds of calcium phosphate ceramics”, *Biomaterials*, vol. 20, pp. 1799-1806, 1999.

[90] Karageorgiou V., Kplan D., “Porosity of 3D biomaterial scaffolds and osteogenesis”, *Biomaterials*, vol.26, pp. 5574-5491, 2005.

[91] Gibson L.J., Ashby M.F., “Cellular Solids: Structure and Properties, 2nd edn.”, *Cambridge University Press*, Cambridge, UK, 1997.

[92] Gaina A., Songb H., Leea B., “Microstructure and mechanical properties of porous yttria stabilized zirconia ceramic using poly methyl methacrylate powder”, *Scripta Materialia*, vol.54, pp. 2081–2085, 2006.

[93] Lorna G., Ashby M., Brendan H., "Cellular Materials in Nature and Medicine", 1st Edition, *Cambridge University Press*, 2010.

[94] Gautam C., Joyner J., Gautam A., Rao J., Vajtai R., "Zirconia based dental ceramics: structure, mechanical properties, biocompatibility and applications", *Dalton Trans.*, vol.45(48), pp. 19194-19215, 2016.

[95] Henkel J., Woodruff M., Epari D., Steck R., Glatt V., Dickinson I., Choong P., Schuetz M., Hutmacher D., "Bone Regeneration Based on Tissue Engineering Conceptions — A 21st Century Perspective", *Bone Research*,pp. 216–248, 2013.

[96] Zuo K., Zeng Y., Jiang D., "Properties of Microstructure-Controllable Porous Yttria-Stabilized Ziroconia Ceramics Fabricated by Freeze Casting", *International Journal of Applied Ceramic Technology*, vol.5, pp. 198–203, 2008.

[97] Santacruz, I., Anapoorani K., Binner J., "Preparation of High Solids Content Nanozirconia Suspensions, *J.Am. Ceram.Soc.*, Vol. 91, pp. 398–405, 2008.

[98] Silva, Angelus G. P., "Capítulo VII: Propriedades Físicas", *Estrutura e Propriedades de Materiais Cerâmicos*, 2015.

[99] Y. M Chiang, D. P Birnie, and W. D Kingery, Physical ceramics., *Wiley*, 1997.

Support Information

Archimedes or immersion method for determination of porosity

Two kinds of porosity can be differentiated: open and closed porosity. Open porosity, $\mathbf{P_o}$, refers to the fraction of the volume of a sample that can be occupied with a fluid. Closed porosity, $\mathbf{P_c}$, refers to the fraction of the total volume of the sample in which fluids flow can't effectively occur and also to the pores isolated inside the sample. Therefore, the total volume of the sample, $\mathbf{V_T}$, is the sum of the actual volume of the solid, $\mathbf{V_s}$, the volume of open pores, $\mathbf{V_{po}}$, and the volume of the closed pores $\mathbf{V_{pc}}$ (see Equation 4).

$$V_T = V_s + V_{po} + V_{pc} \qquad \textbf{Equation 4}$$

The theoretical density of the sample, $\boldsymbol{\rho_t}$, is defined as the ratio between the mass of the solid, $\mathbf{m_1}$, and the volume, **Vs**, occupied by it (see Equation 5).

$$\rho_t = \frac{m_1}{V_s} \qquad \textbf{Equation 5}$$

The apparent volume, $\mathbf{V_a}$, is defined by the sum of the volume of the solid, $\mathbf{V_s}$, and the volume of closed pores, $\mathbf{V_{pc}}$, see Equation 6.

$$V_a = V_s + V_{pc} \qquad \textbf{Equation 6}$$

So, and accordance to Equation 4:

$$V_T = V_a + V_{po} \qquad \textbf{Equation 7}$$

Now if we accept that during the Archimedes method, water wets the entire surface of the sample, the volume of the open pores, $\boldsymbol{V_{po}}$,can be calculated by the ratio between the difference of the impregnated mass, $\mathbf{m_2}$, and the dry mass, $\mathbf{m_1}$, and the water density $\boldsymbol{\rho_{H_2O}}$ (see Equation 8).

$$V_{po} = \frac{m_2 - m_1}{\rho_{H_2O}} \qquad \textbf{Equation 8}$$

$\rho_{H_2O} \approx 1$ g/ cm^3.

The apparent volume ($\mathbf{V_a}$) is given by

$$V_a = \frac{m_1 - m_3}{\rho_{H_2O}} \qquad \textbf{Equation 9}$$

Where $\mathbf{m_3}$ is the mass of the sample when suspended in a liquid (water in this case).

Considering equation 7, V_T , the total volume of the sample is given by

$$V_T = \frac{m_2 - m_3}{\rho_{H_2O}} \qquad \textbf{Equation 10}$$

From the volumes calculated by the method described above, it is possible to determine the open porosity and closed porosity.

The closed ($\mathbf{P_c}$) and open ($\mathbf{P_o}$) porosities can be obtained using the following expressions (see Equations 11 and 12). [98,99]

$$P_c = \frac{V_{pc}}{V_T} \times 100\% \qquad \textbf{Equation 11}$$

$$P_o = \frac{V_{po}}{V_T} \times 100\% \qquad \textbf{Equation 12}$$

X- Ray diffraction data sheets

Following are presented the X-ray diffraction data sheets used to identify zirconia crystalline phases upon XRD characterization.

Name and formula

Reference code:	00-041-1105
Compound name:	Yttrium Oxide
Common name:	yttria
PDF index name:	Yttrium Oxide
Empirical formula:	O_3Y_2
Chemical formula:	Y_2O_3

Crystallographic parameters

Crystal system:	Cubic
Space group:	Ia3
Space group number:	206
a (Å):	10.6041
b (Å):	10.6041
c (Å):	10.6041
Alpha (°):	90.0000
Beta (°):	90.0000
Gamma (°):	90.0000
Calculated density (g/cm^3):	5.03
Volume of cell (10^6 pm^3):	1192.40
Z:	16.00
RIR:	9.10

Subfiles and quality

Subfiles:	Alloy, metal or intermetalic Common Phase Inorganic
Quality:	Star (S)

Comments

Color:	White
Color:	White
Melting Point:	2440 C
Sample Source or Locality:	Sample obtained from Research Chemicals, Phoenix, Arizona, USA
Sample Preparation:	Annealed for 48 hours at 1200 C. Average relative standard deviation in intensity of the ten strongest reflections for three specimen mounts = 2%. Validated by a calculated pattern
Additional Patterns:	To replace 25-1200.

References

Primary reference: Martin, K., McCarthy, G., North Dakota State University, Fargo, North Dakota, USA., *ICDD Grant-in-Aid*, (1989)

Peak list

No.	h	k	l	d [Å]	2Theta[deg]	I [%]
1	2	0	0	5.30700	16.692	1.0
2	2	1	1	4.33000	20.495	13.0
3	2	2	2	3.06100	29.150	100.0
4	3	2	1	2.83500	31.532	1.0
5	4	0	0	2.65100	33.784	24.0
6	4	1	1	2.49900	35.907	5.0
7	4	2	0	2.37150	37.909	1.0
8	3	3	2	2.26050	39.847	6.0
9	4	2	2	2.16450	41.695	1.0
10	4	3	1	2.07880	43.499	8.0
11	5	2	1	1.93570	46.899	2.0
12	4	4	0	1.87400	48.541	39.0
13	4	3	3	1.81830	50.129	2.0
14	6	0	0	1.76770	51.668	1.0
15	6	1	1	1.72000	53.211	5.0
16	6	2	0	1.67670	54.699	1.0
17	5	4	1	1.63610	56.174	4.0
18	6	2	2	1.59840	57.622	25.0
19	6	3	1	1.56330	59.042	5.0
20	4	4	4	1.53040	60.441	4.0
21	5	4	3	1.49950	61.822	2.0
22	6	4	0	1.47050	63.180	1.0
23	7	2	1	1.44300	64.528	3.0
24	6	4	2	1.41700	65.860	1.0
25	6	5	1	1.34670	69.778	2.0
26	8	0	0	1.32550	71.061	4.0
27	8	1	1	1.30520	72.339	3.0
28	8	2	0	1.28590	73.602	2.0
29	6	5	3	1.26740	74.858	2.0
30	6	6	0	1.24960	76.113	1.0
31	8	3	1	1.23270	77.348	3.0
32	6	6	2	1.21630	78.590	6.0
33	7	5	2	1.20070	79.814	1.0
34	8	4	0	1.18560	81.040	4.0
35	8	3	3	1.17110	82.258	1.0
36	8	4	2	1.15700	83.483	1.0
37	9	2	1	1.14350	84.696	2.0
38	6	6	4	1.13050	85.903	1.0
39	8	5	1	1.11780	87.121	2.0
40	9	3	2	1.09380	89.537	2.0
41	8	4	4	1.08230	90.751	4.0
42	9	4	1	1.07120	91.960	2.0
43	10	0	0	1.06040	93.175	1.0
44	10	1	1	1.05000	94.381	1.0
45	10	2	0	1.03990	95.590	3.0
46	9	4	3	1.03000	96.811	1.0
47	10	2	2	1.02040	98.033	3.0
48	10	3	1	1.01110	99.254	2.0
49	8	7	1	0.99320	101.714	2.0
50	10	4	0	0.98450	102.967	2.0

51	10	3	3	0.97620	104.199	1.0
52	10	4	2	0.96800	105.455	2.0
53	9	5	4	0.96010	106.703	1.0
54	11	2	1	0.94480	109.235	2.0
55	8	8	0	0.93740	110.519	1.0
56	10	4	4	0.92310	113.121	1.0
57	11	3	2	0.91600	114.479	1.0
58	10	6	0	0.90930	115.803	1.0
59	11	4	1	0.90270	117.151	1.0
60	10	6	2	0.89630	118.503	2.0
61	9	6	5	0.88970	119.948	1.0

Stick Pattern

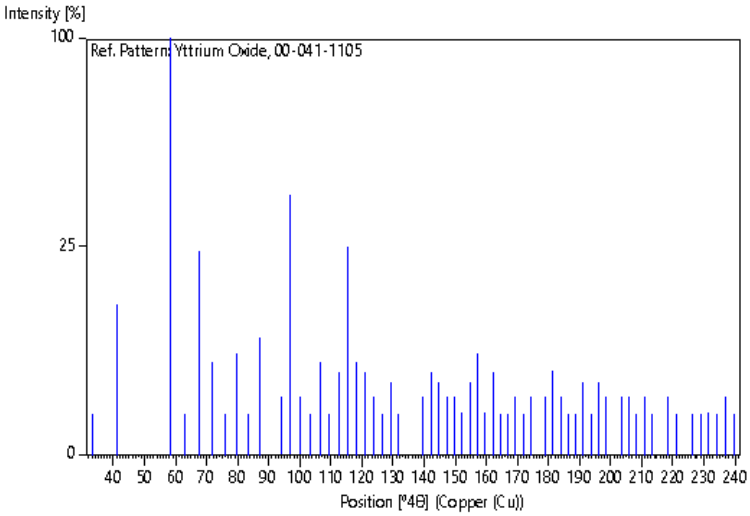

Name and formula

Reference code: 00-042-1164

Compound name: Zirconium Oxide
PDF index name: Zirconium Oxide

Empirical formula: O_2Zr
Chemical formula: ZrO_2

Crystallographic parameters

Crystal system: Tetragonal
Space group: P42/nmc
Space group number: 137

a (Å): 3.6400
b (Å): 3.6400
c (Å): 5.2700
Alpha (°): 90.0000
Beta (°): 90.0000
Gamma (°): 90.0000

Volume of cell (10^6 pm^3): 69.83
Z: 2.00

RIR: -

Status, subfiles and quality

Status: Diffraction data collected at non ambient temperature
Subfiles: Alloy, metal or intermetalic
Common Phase
Corrosion
Forensic
Inorganic
Superconducting Material
Quality: Star (S)

Comments

Temperature of Data Collection: Pattern taken at 1250 C. D-values calculated using cell parameters reported in reference
Additional Patterns: To replace 24-1164
Additional Patterns: See ICSD 23928 (PDF 73-1441).

References

Primary reference: Teufer, G., *Acta Crystallogr.*, **15**, 1187, (1962)

Peak list

No.	h	k	l	d [Å]	2Theta[deg]	I [%]
1	1	0	1	2.99500	29.807	100.0
2	0	0	2	2.63500	33.995	39.0
3	1	1	0	2.57400	34.827	34.0
4	1	0	2	2.13400	42.319	2.0
5	1	1	2	1.84100	49.469	34.0
6	2	0	0	1.82000	50.079	38.0
7	1	0	3	1.58200	58.276	12.0
8	2	1	1	1.55530	59.376	13.0
9	2	0	2	1.49750	61.913	7.0
10	2	1	2	1.38500	67.583	1.0
11	0	0	4	1.31750	71.559	6.0
12	2	2	0	1.28700	73.528	8.0
13	1	0	4	1.23880	76.897	1.0
14	2	1	3	1.19400	80.353	3.0
15	3	0	1	1.18240	81.305	3.0
16	1	1	4	1.17280	82.113	3.0
17	2	2	2	1.15640	83.536	2.0
18	3	1	0	1.15110	84.008	2.0
19	2	0	4	1.06720	92.406	2.0
20	3	1	2	1.05480	93.820	3.0
21	1	0	5	1.01240	99.081	2.0
22	3	0	3	0.99830	100.998	2.0
23	3	2	1	0.99150	101.956	2.0
24	2	2	4	0.92060	113.594	2.0
25	4	0	0	0.91000	115.662	3.0

26	2	1	5	0.88470	121.078	1.0
27	0	0	6	0.87830	122.573	1.0
28	3	2	3	0.87530	123.294	1.0
29	4	1	1	0.87070	124.427	1.0
30	3	1	4	0.86680	125.413	1.0
31	4	0	2	0.86020	127.142	1.0
32	3	3	0	0.85800	127.737	1.0
33	1	1	6	0.83130	135.828	1.0
34	3	3	2	0.81580	141.547	3.0
35	4	2	0	0.81390	142.322	3.0
36	3	0	5	0.79570	150.968	2.0
37	2	0	6	0.79100	153.726	3.0
38	4	1	3	0.78880	155.132	3.0
39	4	2	2	0.77770	164.178	3.0

Stick Pattern

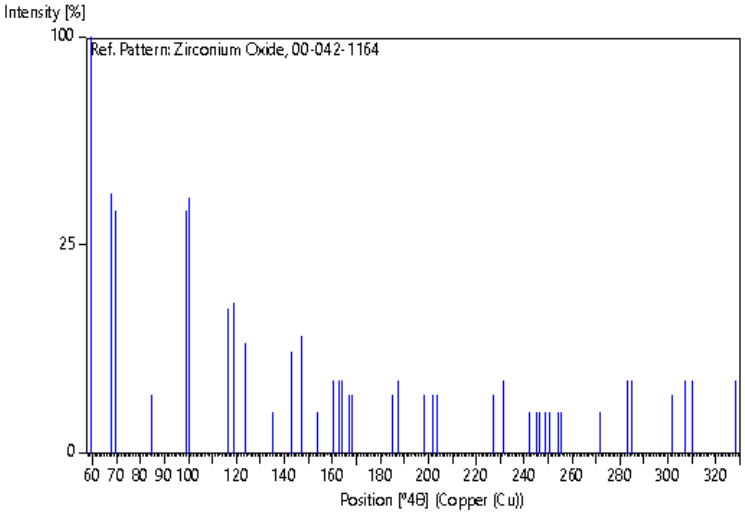

Name and formula

Reference code:	00-037-1484
Mineral name:	Baddeleyite, syn
Compound name:	Zirconium Oxide
Common name:	zirconia
PDF index name:	Zirconium Oxide
Empirical formula:	O_2Zr
Chemical formula:	ZrO_2

Crystallographic parameters

Crystal system:	Monoclinic
Space group:	P21/a
Space group number:	14
a (Å):	5.3129
b (Å):	5.2125
c (Å):	5.1471

Alpha (°):	90.0000
Beta (°):	99.2180
Gamma (°):	90.0000
Volume of cell (10^6 pm^3):	140.70
Z:	4.00
RIR:	2.60

Subfiles and quality

Subfiles:	Alloy, metal or intermetalic Common Phase Corrosion Educational pattern Forensic Inorganic Mineral NBS pattern Superconducting Material
Quality:	Star (S)

Comments

Color:	Colorless
Sample Source or Locality:	Sample was obtained from Titanium Alloy Manufacturing Co. (1990) and was heated to 1300° for 48 hours
Analysis:	Spectrographic analysis showed that this sample contained less than 0.01% each of Al, Hf and Mg and between 0.1 and 0.01% each of Fe, Si and Ti
Structures:	The structure of ZrO_2 (baddeleyite) was determined by McCullough and Trueblood (1) and confirmed by Smith and Newkirk (2). There are a number of polymorphic forms of ZrO_2 stable at different temperatures and pressures
Temperature of Data Collection:	The mean temperature of the data collection was 25.5°
Additional Patterns:	To replace 13-307 and 36-420 and validated by calculated pattern 24-1165. Pattern reviewed by Holzer, J., McCarthy, G., North Dakota State Univ., Fargo, North Dakota, USA, *ICDD Grant-in-Aid* (1990). Agrees well with experimental and calculated patterns. Additional weak reflections [indicated by brackets] were observed
Color:	Colorless
Additional Patterns:	See ICSD 18190 (PDF 72-1669); 15983 (PDF 72-597); 26488 (PDF 74-815); See ICSD 60903 (PDF 78-50).

References

Primary reference:	McMurdie, H., Morris, M., Evans, E., Paretzkin, B., Wong-Ng, W., Hubbard, C., *Powder Diffraction*, **1**, 275, (1986)
Structure:	(2) Smith, D., Newkirk, H., *Acta Crystallogr.*, **18**, 983, (1965)

Peak list

No.	h	k	l	d [Å]	2Theta[deg]	I [%]
1	0	0	1	5.08701	17.419	3.0
2	1	1	0	3.69765	24.048	14.0
3	0	1	1	3.63907	24.441	10.0
4	-1	1	1	3.16470	28.175	100.0
5	1	1	1	2.84063	31.468	68.0
6	2	0	0	2.62268	34.160	21.0
7	0	2	0	2.60618	34.383	11.0
8	0	0	2	2. 0		
9	-2	0	1	2.49945	35.900	2.0
10	-2	1	0	2.34250	38.396	1.0
11	1	2	0	2.33404	38.541	4.0
12	0	1	2	2.28450	39.411	1.0
13	-2	1	1	2.25274	39.990	1.0
14	-1	1	2	2.21377	40.725	12.0
15	2	0	1	2.19188	41.150	5.0
16	-1	2	1	2.18053	41.374	5.0
17	2	1	1	2.02030	44.826	7.0
18	-2	0	2	1.99101	45.522	6.0
19	-2	1	2	1.85933	48.949	2.0
20	2	2	0	1.84810	49.266	18.0
21	0	2	2	1.81874	50.116	22.0
22	-2	2	1	1.80383	50.559	13.0
23	-1	2	2	1.78297	51.193	5.0
24	0	0	3	1.69371	54.104	11.0
25	2	2	1	1.67723	54.680	1.0
26	1	2	2	1.66070	55.270	11.0
27	3	1	0	1.65712	55.400	11.0
28	-3	1	1	1.65245	55.570	9.0
29	0	3	1	1.64394	55.883	6.0
30	-1	1	3	1.61000	57.168	7.0
31	-1	3	1	1.59235	57.861	4.0
32	-2	2	2	1.58220	58.268	3.0
33	1	3	1	1.54586	59.775	8.0
34	-2	0	3	1.53932	60.055	7.0
35	3	1	1	1.50952	61.367	5.0
36	-3	1	2	1.49596	61.984	5.0
37	1	1	3	1.47767	62.838	8.0
38	3	2	0	1.45201	64.079	1.0
39	2	3	0	1.44856	64.250	2.0
40	0	3	2	1.43432	64.966	1.0
41	-2	3	1	1.42616	65.384	2.0
42	0	2	3	1.42006	65.700	6.0
43	-1	3	2	1.41654	65.884	4.0
44	2	3	1	1.36150	68.912	1.0
45	3	2	1	1.34937	69.620	1.0
46	-3	2	2	1.33980	70.190	1.0
47	-2	2	3	1.32534	71.071	2.0
48	-4	0	1	1.32165	71.300	4.0
49	4	0	0	1.31130	71.950	1.0
50	-2	3	2	1.30888	72.104	1.0
51	0	4	0	1.30348	72.450	1.0
52	3	1	2	1.30050	72.642	1.0
53	-3	1	3	1.28622	73.580	1.0
54	0	0	4	1.26995	74.682	2.0
55	1	4	0	1.26469	75.046	4.0
56	-1	1	4	1.24548	76.410	1.0
57	3	3	0	1.23211	77.392	1.0
58	4	0	1	1.22298	78.079	1.0

59	0	3	3	1.21273	78.866	1.0

Stick Pattern

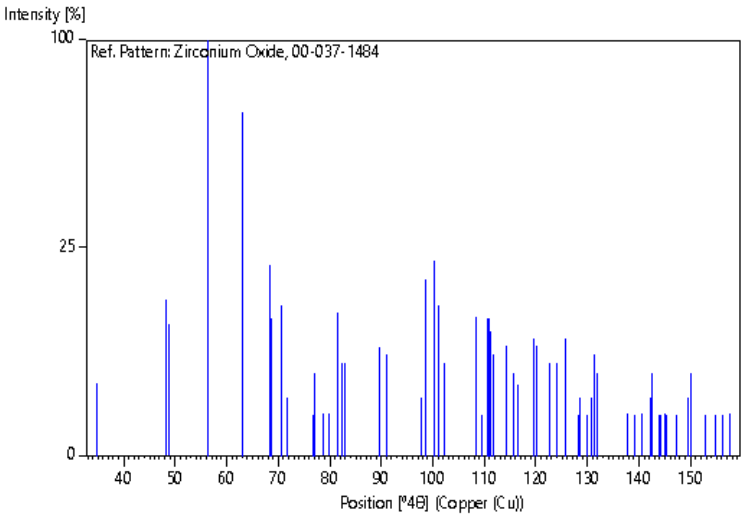

SEM images

- **Sample A:**

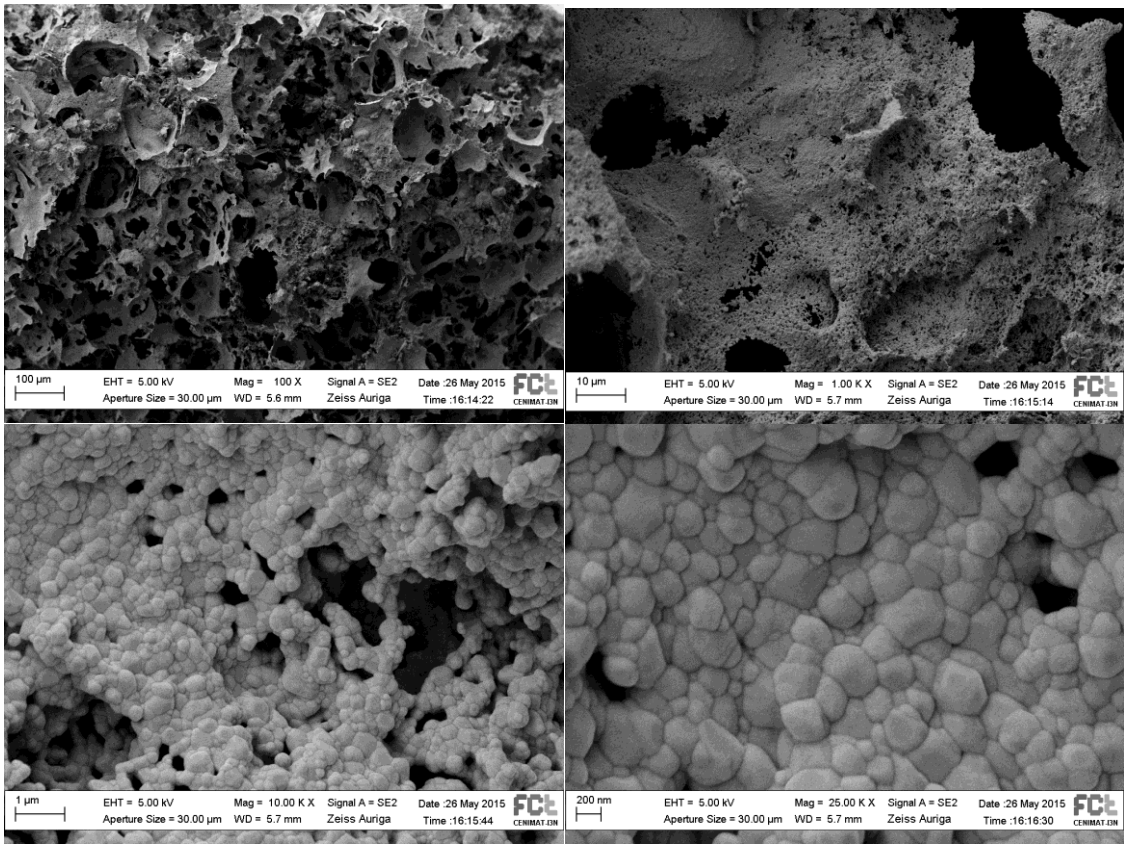

- **Sample B:**

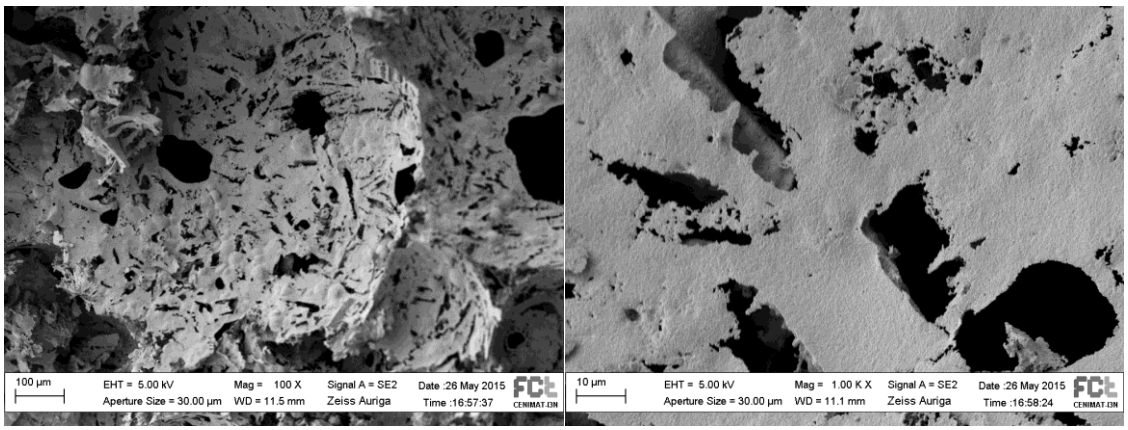

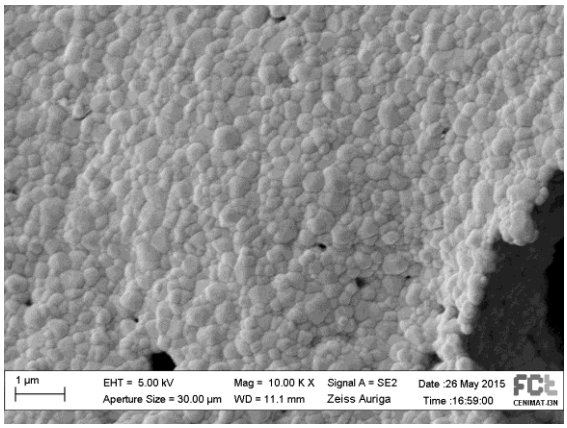
1 µm
EHT = 5.00 kV
Aperture Size = 30.00 µm
Mag = 10.00 K X
WD = 11.1 mm
Signal A = SE2
Zeiss Auriga
Date :26 May 2015
Time :16:59:00

- **Sample C:**

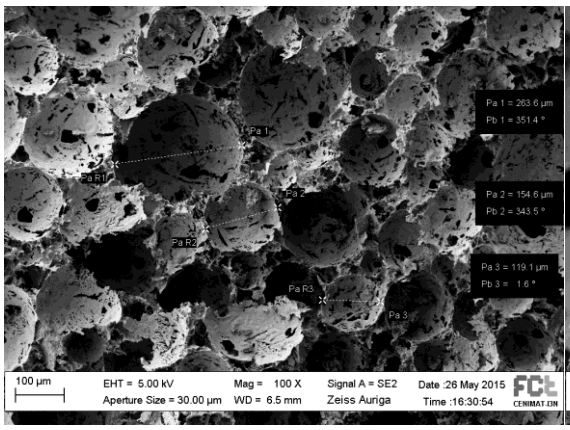
Pa 1 = 263.6 µm
Pb 1 = 351.4 °
Pa 2 = 154.6 µm
Pb 2 = 343.5 °
Pa 3 = 119.1 µm
Pb 3 = 1.6 °
100 µm
EHT = 5.00 kV
Aperture Size = 30.00 µm
Mag = 100 X
WD = 6.5 mm
Signal A = SE2
Zeiss Auriga
Date :26 May 2015
Time :16:30:54

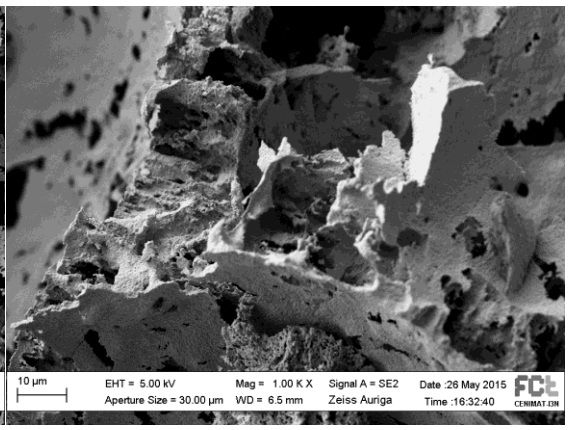
10 µm
EHT = 5.00 kV
Aperture Size = 30.00 µm
Mag = 1.00 K X
WD = 6.5 mm
Signal A = SE2
Zeiss Auriga
Date :26 May 2015
Time :16:32:40

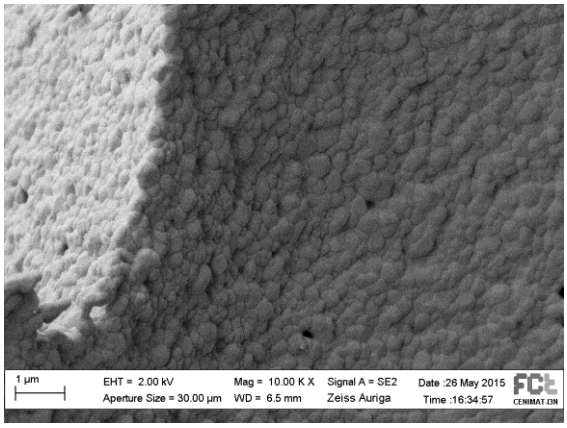
1 µm
EHT = 2.00 kV
Aperture Size = 30.00 µm
Mag = 10.00 K X
WD = 6.5 mm
Signal A = SE2
Zeiss Auriga
Date :26 May 2015
Time :16:34:57

- **Sample D:**

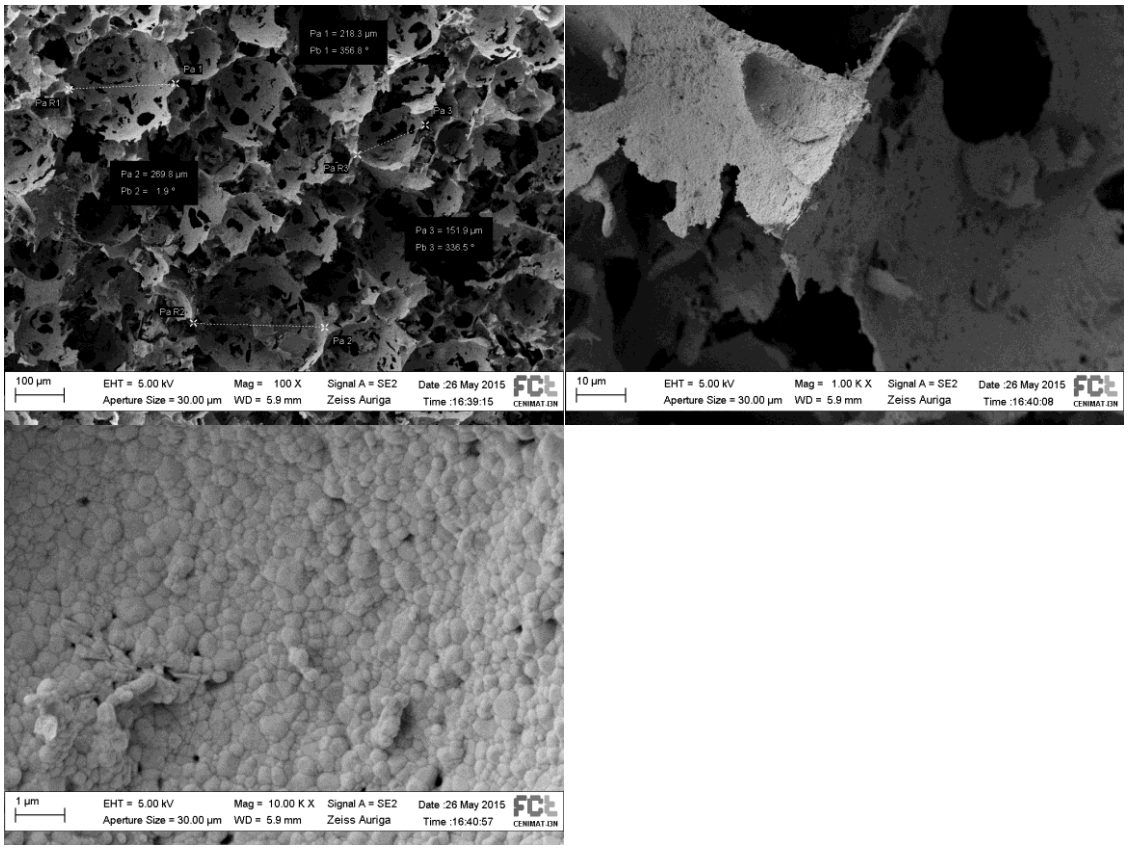

- **Sample E:**

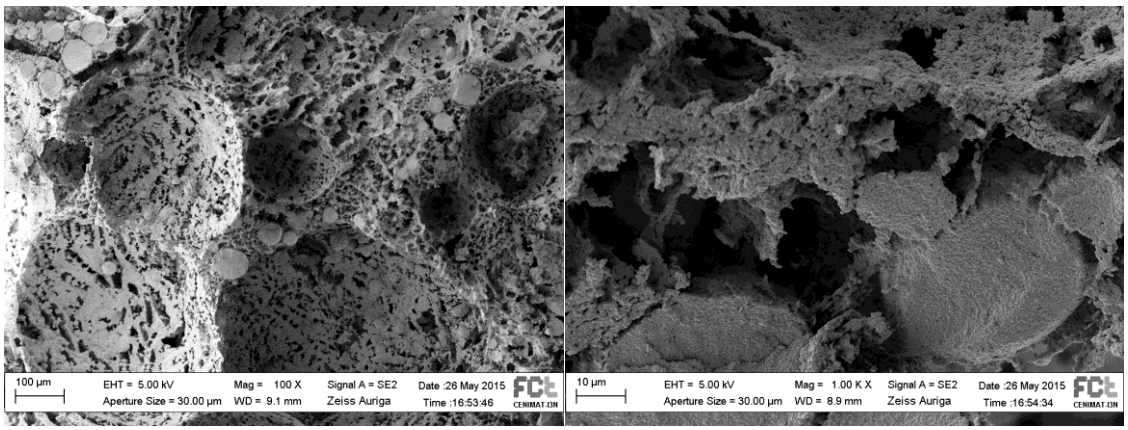

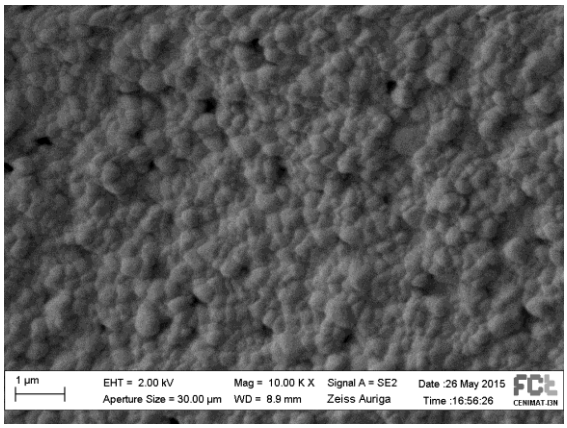
1 µm
EHT = 2.00 kV
Aperture Size = 30.00 µm
Mag = 10.00 K X
WD = 8.9 mm
Signal A = SE2
Zeiss Auriga
Date :26 May 2015
Time :16:56:26
CENIMAT I3N

- **Sample F:**

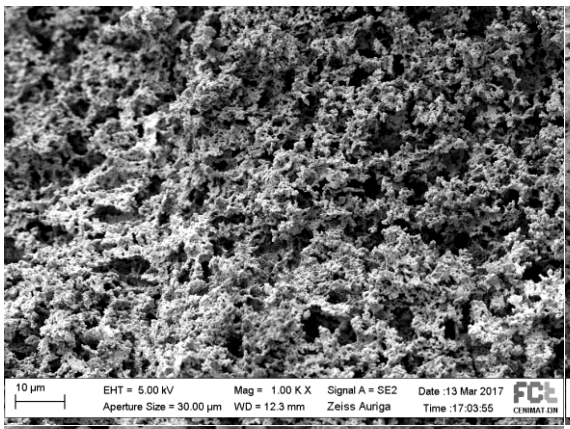
10 µm
EHT = 5.00 kV
Aperture Size = 30.00 µm
Mag = 1.00 K X
WD = 12.3 mm
Signal A = SE2
Zeiss Auriga
Date :13 Mar 2017
Time :17:03:55
CENIMAT I3N

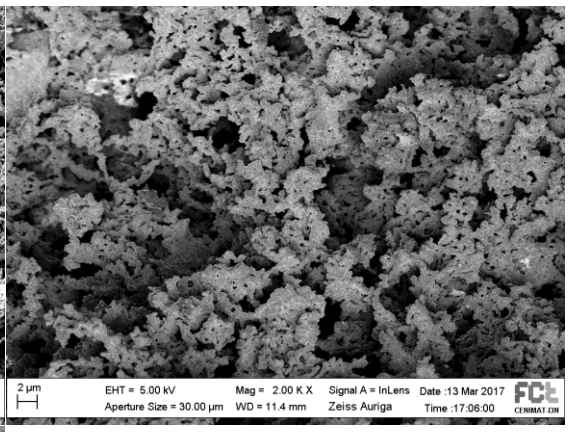
2 µm
EHT = 5.00 kV
Aperture Size = 30.00 µm
Mag = 2.00 K X
WD = 11.4 mm
Signal A = InLens
Zeiss Auriga
Date :13 Mar 2017
Time :17:06:00
CENIMAT I3N

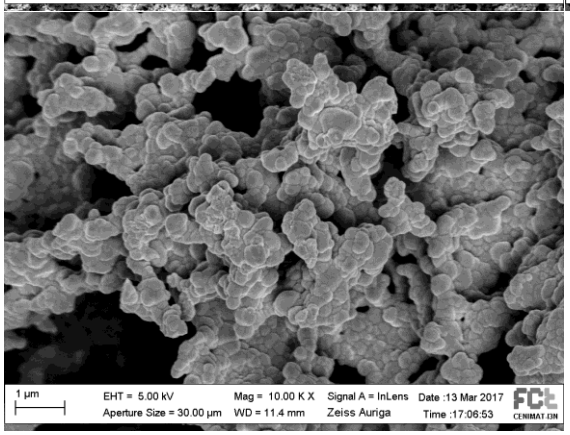
1 µm
EHT = 5.00 kV
Aperture Size = 30.00 µm
Mag = 10.00 K X
WD = 11.4 mm
Signal A = InLens
Zeiss Auriga
Date :13 Mar 2017
Time :17:06:53
CENIMAT I3N

- **Sample G:**

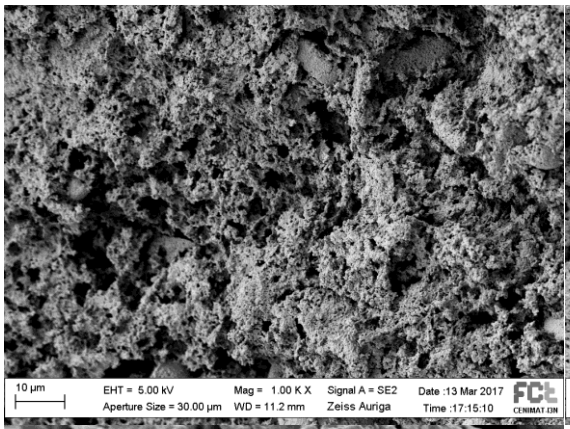
10 µm
EHT = 5.00 kV
Aperture Size = 30.00 µm
Mag = 1.00 K X
WD = 11.2 mm
Signal A = SE2
Zeiss Auriga
Date :13 Mar 2017
Time :17:15:10

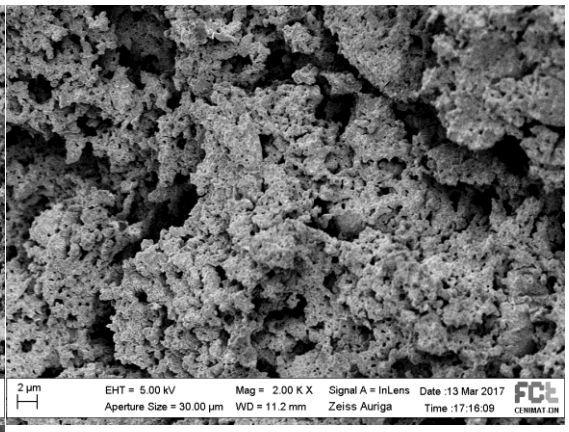
2 µm
EHT = 5.00 kV
Aperture Size = 30.00 µm
Mag = 2.00 K X
WD = 11.2 mm
Signal A = InLens
Zeiss Auriga
Date :13 Mar 2017
Time :17:16:09

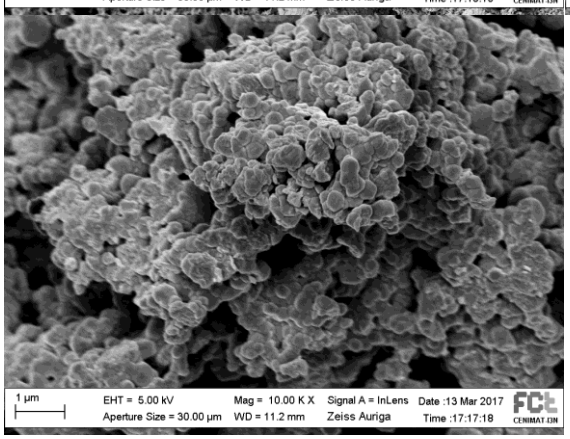
1 µm
EHT = 5.00 kV
Aperture Size = 30.00 µm
Mag = 10.00 K X
WD = 11.2 mm
Signal A = InLens
Zeiss Auriga
Date :13 Mar 2017
Time :17:17:18